BRINT: Binary Rotation Invariant and Noise Tolerant Texture Classification

Li Liu, *Member, IEEE*, Yunli Long, Paul W. Fieguth, *Member, IEEE*, Songyang Lao, and Guoying Zhao, *Senior Member, IEEE*

***Abstract*— In this paper, we propose a simple, efficient, yet robust multiresolution approach to texture classification—binary rotation invariant and noise tolerant (BRINT). The proposed approach is very fast to build, very compact while remaining robust to illumination variations, rotation changes, and noise. We develop a novel and simple strategy to compute a local binary descriptor based on the conventional local binary pattern (LBP) approach, preserving the advantageous characteristics of uniform LBP. Points are sampled in a circular neighborhood, but keeping the number of bins in a single-scale LBP histogram constant and small, such that arbitrarily large circular neighborhoods can be sampled and compactly encoded over a number of scales. There is no necessity to learn a texton dictionary, as in methods based on clustering, and no tuning of parameters is required to deal with different data sets. Extensive experimental results on representative texture databases show that the proposed BRINT not only demonstrates superior performance to a number of recent state-of-the-art LBP variants under normal conditions, but also performs significantly and consistently better in presence of noise due to its high distinctiveness and robustness. This noise robustness characteristic of the proposed BRINT is evaluated quantitatively with different artificially generated types and levels of noise (including Gaussian, salt and pepper, and speckle noise) in natural texture images.**

***Index Terms*— Texture descriptors, rotation invariance, local binary pattern (LBP), feature extraction, texture analysis.**

I. Introduction

TEXTURE is a fundamental characteristic of the appearance of virtually all natural surfaces and is ubiquitous in natural images. Texture classification, as one of the major problems in texture analysis, has received considerable attention during the past decades due to its value both in understanding how the texture recognition process works in humans as well as in the important role it plays in the field of computer vision and pattern recognition [1]. Typical applications of texture classification include medical image analysis and understanding, object recognition, content-based image retrieval, remote sensing, industrial inspection, and document classification.

The texture classification problem is conventionally divided into the two subproblems. It is generally agreed that the extraction of powerful texture features is of more importance to the success of texture classification and, consequently, most research in texture classification focuses on the feature extraction part [1], with extensive surveys [1]. Nevertheless it remains a challenge to design texture features which are computationally efficient, highly discriminative and effective, robust to imaging environment changes (including changes in illumination, rotation, view point, scaling and occlusion) and insensitive to noise.

Recently, the Bag-of-Words (BoW) paradigm, representing texture images as histograms over a discrete vocabulary of local features, has proved effective in providing texture features [2]–[7]. Representing a texture image using the BoW model typically involves the following three steps:

(i) Local texture descriptors: extracting distinctive and robust texture features from local regions;
(ii) Texton dictionary formulation: generating a set of representative vectors (*i.e.,* textons or dictionary atoms) learned from a large number of texture features;
(iii) Global statistical histogram computation: representing a texture images statistically as a compact histogram over the learned texton dictionary.

Within the BoW framework, the focus of attention has been on the design of local texture descriptors capable of achieving local invariance [2], [4]–[7]. These descriptors can be classified as dense or sparse, with the sparse approaches, such as SPIN, SIFT and RIFT [4], [10], requiring a process of detecting salient regions before applying the texture descriptors, leading to issues of implementation and computational complexity and instability. In contrast, dense approaches, applying texture descriptors pixel by pixel are more popular. Important dense textures descriptors include Gabor wavelets [8], LM filters [5], MR8 filters [5], BIF features [7], LBP [2], Patch descriptor [6] and RP random features [3] and many others [4].

Among local texture descriptors, LBP [2], [11] has emerged as one of the most prominent and has attracted increasing attention in the field of image processing and computer vision

Manuscript received January 10, 2013; revised April 16, 2014; accepted May 10, 2014. Date of publication May 20, 2014; date of current version June 11, 2014. This work was supported in part by the National Natural Science Foundation of China under Contract 61202336 and in part by the Doctoral Fund of Ministry of Education of China under Contract 20124307120025. The associate editor coordinating the review of this manuscript and approving it for publication was Prof. Aleksandra Pizurica.

L. Liu and S. Lao are with the Key Laboratory of Information System Engineering, School of Information System and Management, National University of Defense Technology, Changsha 410073, China (e-mail: dreamliu2010@gmail.com; laosongyang@vip.sina.com).

Y. Long is with the School of Electronic Science and Engineering, National University of Defense Technology, Changsha 410073, China (e-mail: feiyunlyi@126.com).

P. Fieguth is with the Department of Systems Design Engineering, University of Waterloo, Waterloo, ON N2L 3G1, Canada (e-mail: pfieguth@uwaterloo.ca).

G. Zhao is with the Center for Machine Vision Research, Department of Computer Science and Engineering, University of Oulu, Oulu 90014, Finland (e-mail: gyzhao@ee.oulu.fi).

Color versions of one or more of the figures in this paper are available online at http://ieeexplore.ieee.org.

Digital Object Identifier 10.1109/TIP.2014.2325777

due to its outstanding advantages: (1) ease of implementation, (2) no need for pre-training, (3) invariance to monotonic illumination changes, and (4) low computational complexity, making LBP a preferred choice for many applications. Although originally proposed for texture analysis, the LBP method has been successfully applied to many diverse areas of image processing: dynamic texture recognition, remote sensing, fingerprint matching, visual inspection, image retrieval, biomedical image analysis, face image analysis, motion analysis, edge detection, and environment modeling [12]–[17]. Consequently many LBP variants are present in the recent literature.[1]

Although significant progress has been made, most LBP variants still have prominent limitations, mostly the sensitivity to noise [19], [21], and the limiting of LBP variants to three scales, failing to capture long range texture information [19], [21], [23]. Although some efforts have been made to include complementary filtering techniques [21], [24], these *increase* the computational complexity, running counter to the computational efficiency property of the LBP method.

In this paper, we propose a novel, computationally simple approach, the Binary Rotation Invariant and Noise Tolerant (BRINT) descriptor, which has the following outstanding advantages: It is highly discriminative, has low computational complexity, is highly robust to noise and rotation, and allows for compactly encoding a number of scales and arbitrarily large circular neighborhoods. At the feature extraction stage there is no pre-learning process and no additional parameters to be learned.

We derive a rotation invariant and noise tolerant local binary pattern descriptor, dubbed as $\text{BRINT\_S}_{r,q}$, based on a circularly symmetric neighbor set of $8q$ members on a circle of radius r. Parameter q controls the quantization of the angular space, and r determines the spatial scale of the $\text{BRINT\_S}_{r,q}$ operator, which produces a histogram feature of constant dimensionality at any spatial scale r with arbitrary large number of sampling points $8q$ for each texture image.

Motivated by the recent CLBP approach, which was proposed by Guo *et al.* [25] to include both the signs and the magnitudes components between a given central pixel and its neighbors and the center pixel intensity in order to improve the discriminative power of the original LBP operator, we extend BRINT to include a magnitude component and to code the intensity of the center pixel. Based on these methods we develop a discriminative and robust combination for multiresolution analysis, which will be demonstrated experimentally to perform robustly against changes in gray-scale, rotation, and noise without suffering any performance degradation under noise-free situations.

The remainder of this paper is organized as follows. A brief review of LBP and CLBP is given in Section II. Section III presents the motivation and the development of the new proposed BRINT approach in detail, as well as the multiresolution analysis and a brief overview of the classification process. Comprehensive experimental results and comparative evaluation are given in Section IV. Section V concludes the paper. A preliminary version of this work appeared in [9].

[1]A comprehensive bibliography of LBP methodology can be found at http://www.cse.oulu.fi/MVG/LBP_Bibliography/.

II. LBP AND CLBP

Despite the great success of LBP in computer vision and image processing, the original LBP descriptor [11] has some limitations: producing long histograms which are not rotation invariant; capturing only the very local texture structure and being unable to exploit long range information; limited discriminative capability based purely on local binarized differences; and and lacking noise robustness. On the basis of these issues, many LBP variations have been developed (see surveys [12], [13]), focusing on different aspects of the original LBP descriptor.

Dimensionality Reduction and Rotation Invariance

Most common is to reduce the feature length based on some rules, where influential work has been done by Ojala *et al.* [2] who proposed three important descriptors: rotation invariant LBP (LBP^{ri}), uniform LBP (LBP^{u2}), and rotation invariant uniform LBP (LBP^{riu2}). Of these, LBP^{riu2}, described in Section II-A, has become the most popular since it reduces the dimensionality of the original LBP significantly and achieves improved discriminative ability.

Discriminative Power

There are two approaches to improve discriminative power: reclassifying the original LBP patterns to form more discriminative clusters, or including other local binary descriptors. Noticeable examples include the Hamming LBP [26], which regroups nonuniform patterns based on Hamming distance instead of collecting them into a single bin as LBP^{riu2} does, the CLBP approach [25] which is discussed in Section II-B, and the Extended LBP approach [27] which considers the local binary descriptors computed from local intensities, radial differences and angular differences.

Noise Robustness

Ahonen *et al.* introduced Soft LBP (SLBP) method [28] which allows multiple local binary patterns to be generated at each pixel position, to make the traditional LBP approach more robust to noise; however, SLBP is computationally expensive and is no longer strictly invariant to monotonic illumination changes. Tan and Triggs [29] introduced local ternary patterns (LTP), where the binary LBP code ia replaced by a ternary LTP code. The LTP method is more resistant to noise, but no longer strictly invariant to gray-scale changes. Liao *et al.* [21] proposed to use dominant LBP (DLBP) patterns which considers the most frequently occurred patterns in a texture image. The Median Binary Pattern (MBP) proposed in [30] claims increased robustness to impulse noise such as salt-and-pepper noise, but MBP was only explored in a local 3×3-patch. Fathi *et al.* [18] proposed a noise tolerant method based on the traditional LBP by combining a circular majority voting filter and a new LBP variant which regroups the nonuniform LBP patterns in order to gain more discriminability. Raja *et al.* [22] proposed Optimized Local Ternary Patterns (OLTP) based on LTP in order to reduce feature dimensionality, however the authors did not extend OLTP to multiscale analysis. Ren *et al.* [20] proposed a much more efficient Noise Resistant Local Binary Pattern (NRLBP)

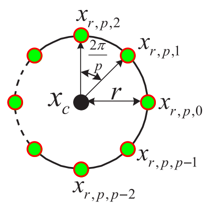

Fig. 1. The (r, p) neighborhood type used to derive a LBP like operator: central pixel and its p circularly and evenly spaced neighbors on circle of radius r.

approach based on the SLBP method, but it is computationally expensive to generalize to larger scales with a bigger number neighboring points.

Combining with Other Approaches

Ojala *et al.* [2] proposed a local contrast descriptor VAR to combine with LBP; It was recommended in [21] that Gabor filters and LBP-based features are mutually complementary because LBP captures the local texture structure, whereas Gabor filters extract global texture information. Ahonen *et al.* proposed an approach named LBP histogram Fourier features (LBP-HF) [24], which combines the LBP and the discrete Fourier transform (DFT). Khellah [19] introduced a Dominant Neighborhood Structure (DNS) method which extracts global rotation-invariant features from the detected image dominant neighborhood structure to complement LBP.

A. Local Binary Patterns (LBP)

The original LBP method, proposed by Ojala *et al.* [11] in 1996, characterizes the spatial structure of a local image texture by thresholding a 3×3 square neighborhood with the value of the center pixel and considering only the sign information to form a local binary pattern. A more general formulation defined on circular symmetric neighborhood systems was proposed in [2] that allowed for multi-resolution analysis and rotation invariance. Formally, given a pixel x_c in the image, the LBP pattern is computed by comparing its value with those of its p neighboring pixels

$$\underline{\boldsymbol{x}}_{r,p} = [x_{r,p,0}, \ldots, x_{r,p,p-1}]^T$$

that are evenly distributed in angle on a circle of radius r centered at center x_c, as in Fig. 1, such that the LBP response is calculated as

$$\mathrm{LBP}_{r,p} = \sum_{n=0}^{p-1} s(x_{r,p,n} - x_c)2^n, \quad s(x) = \begin{cases} 1 & x \geq 0 \\ 0 & x < 0 \end{cases} \tag{1}$$

where $s()$ is the sign function. Relative to the origin at $(0, 0)$ of the center pixel x_c, the coordinates of the neighbors are given by $-r\sin(2\pi n/p), r\cos(2\pi n/p)$. The gray values of neighbors which do not fall exactly in the center of pixels are estimated by interpolation.

Given an $N \times M$ texture image $\mathbf{I}$, a LBP pattern $LBP_{r,p}(i, j)$ can be the computed at each pixel (i, j). A texture image can be characterized by the probability distribution of the LBP patterns. Formally, the whole textured image $\mathbf{I}$ is represented by a LBP histogram vector $\underline{\boldsymbol{h}}$:

$$\underline{\boldsymbol{h}}(k) = \sum_{i=1}^{N}\sum_{j=1}^{M} \delta(\mathrm{LBP}_{r,p}(i, j) - k) \tag{2}$$

TABLE I

NUMBER OF PATTERNS OF DIFFERENT DESCRIPTORS. THE NOTATION CLBP_CSM IS THE ABBREVIATION FOR CLBP_CS$^{riu2}_{r,p}$M$^{riu2}_{r,p}$. THE SAMPLING SCHEMES FOR SCALES 4 AND 5 HAVE BEEN IMPLEMENTED BY ZHAO *et al.* [35] IN THEIR CLBC_CSM APPROACH

Scale	(r, p)	$\mathrm{LBP}_{r,p}$	$\mathrm{LBP}^{ri}_{r,p}$	$\mathrm{LBP}^{riu2}_{r,p}$	CLBP_CSM
Scale 1	$(1, 8)$	256	36	10	200
Scale 2	$(2, 16)$	65536	4116	18	648
Scale 3	$(3, 24)$	16777216	699252	26	1352
Scale 4	$(4, 32)$	2^{32}	huge	34	2312
Scale 5	$(5, 40)$	2^{40}	huge	42	3528
Scale 1-5		infeasible	infeasible	106	8040

where $0 \leq k < d = 2^p$ is the number of LBP patterns. To be able to include textural information at different scales, the LBP operator was later extended to use neighborhoods of different sizes [2], with values of (r, p) selected as $(1, 8), (2, 16), (3, 24), \ldots, (r, 8r)$.

A rotation invariant version $\mathrm{LBP}^{ri}_{r,p}$ of the original $\mathrm{LBP}_{r,p}$ descriptor was proposed by Pietikäinen *et al.* in [34]. The $\mathrm{LBP}^{ri}_{r,p}$ descriptor uses only the rotation invariant LBP patterns

$$\mathrm{LBP}^{ri}_{r,p} = \min\{ROR(\mathrm{LBP}_{r,p}, i) \;\mid\; i = 0, 1, \ldots, p-1\} \tag{3}$$

where $ROR(x, i)$ performs a circular i-step bit-wise right shift on x, i times. Keeping only those rotationally-unique patterns leads to a significant reduction in feature dimensionality, as shown in Table I, although beyond one scale the number of bins remains large. The $\mathrm{LBP}^{ri}_{r,p}$ descriptor was found to have poor performance [2], [34], therefore it has received little attention.

In order to obtain improved rotation invariance and to further reduce the dimensionality of the LBP histogram feature, building on $\mathrm{LBP}^{ri}_{r,p}$ Ojala *et al.* [2] proposed the "rotation invariant uniform" patterns $\mathrm{LBP}^{riu2}_{r,p}$, the collection of those rotation invariance patterns having a U value of at most 2:

$$\mathrm{LBP}^{riu2}_{r,p} = \begin{cases} \sum_{n=0}^{p-1} s(x_{r,p,n} - x_c), & \text{if } U(\mathrm{LBP}_{r,p}) \leq 2 \\ p+1, & \text{otherwise} \end{cases} \tag{4}$$

where

$$U(\mathrm{LBP}_{r,p}) = \sum_{n=0}^{p-1} |s(x_{r,p,n} - x_c) - s(x_{r,p,n+1} - x_c)|. \tag{5}$$

There are $p + 1$ distinct groups of rotation invariant uniform patterns, with the rest considered as "nonuniform" patterns which are merged into one group, leading to a much lower dimensional histogram representation for the whole image, as shown in Table I. The success of the $\mathrm{LBP}^{riu2}_{r,p}$ operator comes from the experimental observation that the uniform patterns appear to be fundamental properties of local image textures [2], representing salient local texture structure.

Compared with the original $\mathrm{LBP}_{r,p}$ descriptor and its rotation invariant version $\mathrm{LBP}^{ri}_{r,p}$, $\mathrm{LBP}^{riu2}_{r,p}$ has improved rotation invariance, considerably lower dimensionality, and very satisfactory discriminative power which make it attractive [2], [25].

B. Completed Local Binary Patterns (CLBP)

Completed Local Binary Patterns (CLBP) [25] consist of three LBP-like descriptors: CLBP_C, CLBP_S and CLBP_M which include information on the center pixel, signed differences, and magnitudes of differences, respectively, with the variants tested to improve the discriminative power of the original LBP operator. The CLBP_S descriptor is exactly the same as the original LBP descriptor; CLBP_C thresholds the central pixel against the global mean gray value of the whole image: $\text{CLBP\_C} = s(x_c - \frac{1}{MN}\sum_{i=1}^{N}\sum_{j=1}^{M}\mathbf{I}(i,j))$. CLBP_M performs a binary comparison between the absolute value of the difference between the central pixel and its neighbors and a global threshold to generate an LBP-like code:

$$\text{CLBP\_M}_{r,p} = \sum_{n=0}^{p-1} s(|x_{r,p,n} - x_c| - \mu_{r,p}^{g})2^n \tag{6}$$

where the global threshold $\mu_{r,p}^{g}$ used by Guo *et al.* [25] is computed as:

$$\mu_{r,p}^{g} = \frac{\sum_{i=r+1}^{N-r}\sum_{j=r+1}^{M-r}\sum_{n=0}^{p-1}|x_{r,p,n}(i,j) - x(i,j)|}{(M-2r)(N-2r)p} \tag{7}$$

Since the CLBP approach adopts the 'uniform and rotation invariant' scheme for texture representation, clearly it inherits the main characteristics of the traditional $\text{LBP}_{r,p}^{riu2}$ (*i.e.* $\text{CLBP\_S}_{r,p}^{riu2}$) descriptor. Moreover, due to the combination of three complementary descriptors $\text{CLBP\_M}_{r,p}^{riu2}$, CLBP_C and $\text{CLBP\_S}_{r,p}^{riu2}$ jointly, CLBP has provided better texture classification performance than traditional $\text{LBP}_{r,p}^{riu2}$, but leads to much higher dimensionality.

III. BRINT: A Binary Rotation Invariant and Noise Tolerant Descriptor

A. Motivation

Although the original LBP approach is attractive for its conceptual simplicity and efficient computation, a straightforward application of the original $\text{LBP}_{r,p}$ histogram features is limited:

(1) As shown in Table I, the original LBP operator produces rather long histograms (2^p distinct values), overwhelmingly large even for small neighborhoods, leading to poor discriminant power and large storage requirements.
(2) The LBP operator captures only the very local structure of the texture, appropriate for micro-textures but not for macro-textures. Because the LBP dimensionality becomes intractable as the sampling radius increases, it is difficult to collect information from a larger area.
(3) The original LBP codes computed based on (1) are sensitive to image rotation.
(4) LBP codes can be highly sensitive to noise: the slightest fluctuation above or below the value of the central pixel is treated the same way as a major contrast.

The rotation invariant descriptor $\text{LBP}_{r,p}^{ri}$ has received very limited attention, having shortcomings (1,2,4) listed above and in fact providing poor results for rotation invariant texture classification [34].

The $\text{LBP}_{r,p}^{riu2}$ descriptor has avoided the disadvantages (1) and (2), which can be seen from Table I. However despite its clear advantages of dimensionality, gray scale and rotation invariance, and suitability for multi-resolution analysis, it suffers in terms of reliability and robustness as it only uses the uniform patterns and has minimal tolerance to noise.

The $\text{CLBP\_C} * \text{CLBP\_S}_{r,p}^{riu2} * \text{CLBP\_M}_{r,p}^{riu2}$, abbreviated as CLBP_CSM, has been shown to perform better than $\text{LBP}_{r,p}^{riu2}$ [25], due to the joint behavior of the three complementary LBP-like codes CLBP_C, CLBP_S and CLBP_M, although this concatenation leads to a feature vector relatively high dimensionality (Table I). In standard CLBP_CSM applications, typically three scales are considered, with a corresponding dimensionality of 2200. The CLBP_CSM approach adopted in [35], utilizes five scales to extract texture feature, leading to an even higher dimensionality of 8040. For a multi-resolution analysis, with non-local features based on a larger number of scales, the increased dimensionality leads to challenges in storage and reliable classifier learning.

All of the discussed descriptors share one or more weaknesses of noise sensitivity, high dimensionality, and/or information insufficiency. Though all of the LBP-based approaches are computationally simple at the feature extraction step, except for $\text{LBP}_{r,p}^{riu2}$ the other descriptors are all computationally expensive at the *classification* stage due to the high dimensionality of the histogram feature vector. The inherent difficulty in extracting suitable features for robust texture classification lies in balancing the three competing goals of discriminativeness, low computational requirements, and a robustness to noise. The goal of this paper was to build on the advantageous characteristics of LBP, developing an approach which achieves a better balance among these three competing requirements, in particular increasing robustness to noise. Our concern with the reduced approaches of LBP^{riu2} and CLBP_CSM lies with the use of only the uniform LBP patterns, which appear to lack texture discriminability. Instead, the LBP^{ri}, although having large dimensionality, possesses meaningful texture features and strikes us as a more promising starting point.

B. BRINT: Proposed Approach

1) BRINT_S Descriptor: The construction of the local BRINT_S descriptor is illustrated in Fig. 2. Similar to the sampling scheme in the original LBP approach, we sample pixels around a central pixel x_c, however on any circle of radius r we restrict the number of points sampled to be a multiple of eight, thus $p = 8q$ for positive integer q. So the neighbors of x_c sampled on radius r are $\underline{\boldsymbol{x}}_{r,8q} = [x_{r,8q,0}, \ldots, x_{r,8q,8q-1}]^T$.

In contrast to original LBP, we transform the neighbor vector $\underline{\boldsymbol{x}}_{r,8q}$ by local averaging along an arc,

$$y_{r,q,i} = \frac{1}{q}\sum_{k=0}^{q-1} x_{r,8q,(qi+k)}, \quad i = 0, \ldots, 7, \tag{8}$$

as illustrated in Fig. 2, such that the number of neighbors in $\underline{\boldsymbol{y}}_{r,q}$ is always eight.

Given $\underline{\boldsymbol{y}}_{r,q} = [y_{r,q,0}, \ldots, y_{r,q,7}]^T$, we can trivially compute a binary pattern with respect to the center pixel, as in LBP:

$$\text{BNT\_S}_{r,q} = \sum_{n=0}^{7} s(y_{r,q,n} - x_c)2^n \tag{9}$$

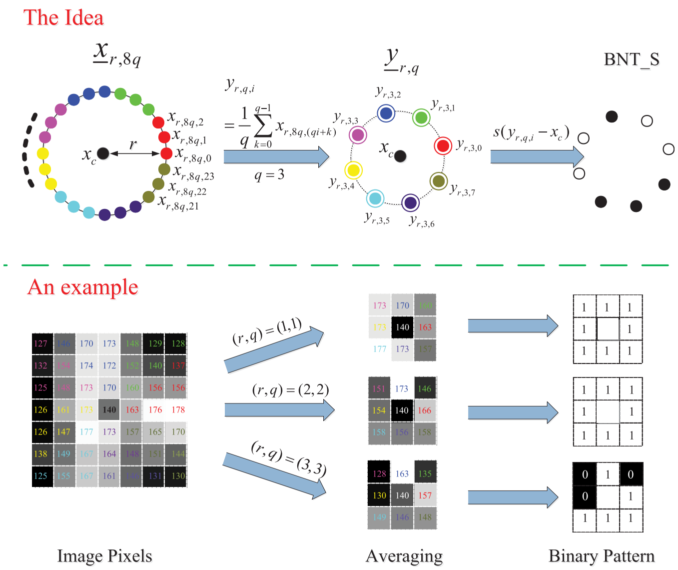

Fig. 2. Illustration of the proposed BNT_S descriptor which is designed to derive the proposed BRINT descriptor: The definition of the BNT_S descriptor, and a 3-scale example illustrating the construction of the proposed BNT_S descriptor. This figure is better read in color. Rather than directly subtracting the gray value x_c of the center pixel from the precise gray value of each neighboring pixel $x_{r,8q,i}, i = 0, \ldots, 8q-1$, the proposed approach introduces a novel idea – Average-Before-Quantization (ABQ) – first transforming the original neighborhood into a new one $y_{r,8q,i}, i = 0, \ldots, 7$, and then thresholding $y_{r,8q,i}, i = 0, \ldots, 7$ at the gray value of the center pixel to generate a binary pattern. See text for further details.

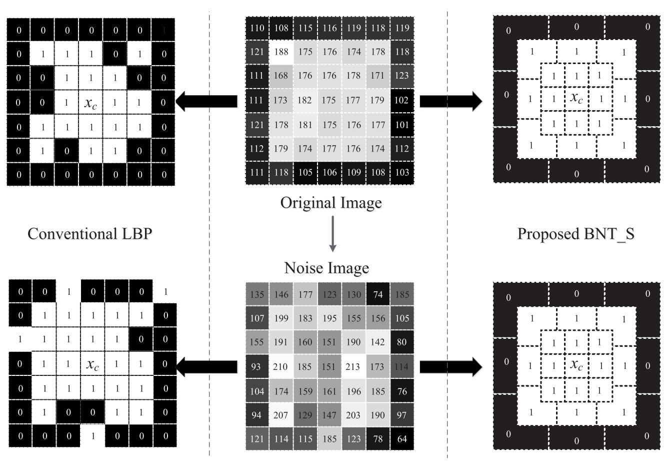

Fig. 3. A motivational example for illustration of noise robustness. Middle: A 7×7-pixels image and its zero mean additive Gaussian noise added version. The conventional LBP responses are shown on the left, in contrast to the BNT_S pattern on the right. The BNT_S approach shows greater consistency in the presence of noise.

where BNT_S represents "Binary Noise Tolerant Sign". One can easily see that for any parameter pair (r, q) there are $2^8 = 256$ BNT_S$_{r,q}$ binary patterns in total. Furthermore, the transformation from $\underline{\boldsymbol{x}}_{r,8q}$ to $\underline{\boldsymbol{y}}_{r,q}$ makes the pattern more robust to noise, as is illustrated in an example in Fig. 3.

As rotation invariance is one of our stated objectives, and to avoid the limitations [13], [19], [21] of uniform patterns, we follow the inspiration of LBP$^{ri}_{r,q}$, grouping equal versions of binary representations under rotations, assigning code numbers to the resulting groups. Formally, then, BRINT_S$_{r,q}$ is

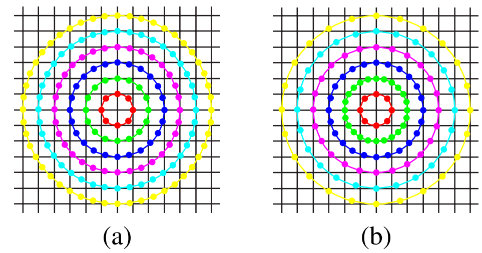

Fig. 4. Illustration of two sampling schemes on an example patch of size 13×13-pixels used in this work: (a) Sampling Scheme 1: $(r, p) \in \{(1, 8), (2, 16), (3, 24), \ldots, (r, 8r)\}$, and (b) Sampling Scheme 2: $(r, p) \in \{(1, 8), (2, 24), (3, 24), \ldots, (r, 24)\}$. The proposed BRINT method using Sampling Scheme 1 or 2 is denoted as BRINT1 or BRINT2, respectively.

defined as

$$\text{BRINT\_S}_{r,q} = \min\{ROR(\text{BNT\_S}_{r,q}, i) | i = 0, \ldots, 7\}, \quad (10)$$

where rotation function $ROR(\bullet, \bullet)$ is as in (3), reducing the number of histogram bins, for one scale, from 256 to 36. The motivation, then, for fixing the number of points in $\underline{\boldsymbol{y}}_{r,q}$ to a constant 8 was to limit the growth in histogram bins with scale.

In terms of parameter q, which controls the number of neighbors being sampled and averaged, we illustrate two reasonable sampling schemes in Fig. 4. Scheme 1, employed in BRINT1, should be more robust to noise, due to having more neighbors to average, however it may cause over-smoothing relative to Scheme 2, employed in method BRINT2.

Fig. 5 validates the basic behavior of BRINT_S$_{r,q}$ as a function of the number of scales by contrasting its classification performance with that of the conventional LBP$^{ri}_{r,p}$ descriptor. The classification results show a significant jump in classification performance on the three Outex databases, outperforming the *best* results reported by Ojala *et al.* [2].

In terms of computation cost, the proposed BRINT_S descriptor does not imply an increase in complexity over the traditional LBP$^{riu2}_{r,p}$. In particular, BRINT_S always deals with local binary patterns based on 8 points, whereas for LBP$^{riu2}_{r,p}$ the mapping from LBP to LBP$^{riu2}_{r,p}$ requires a large lookup table having 2^p elements.

2) BRINT_M Descriptor: Motivated by the striking classification results achieved by BRINT_S and considering the better performance of the CLBP_CSM feature over the single feature LBP$^{riu2}_{r,p}$ proposed by Guo *et al.* [25], we would like to further capitalize on the CLBP_M descriptor by proposing BRINT_M.

Given a central pixel x_c and its p neighboring pixels $x_{r,p,0}, \ldots, x_{r,p,p-1}$, as before in Fig. 2, we first compute the absolute value of the local differences between the center pixel x_c and its neighbors

$$\Delta_{r,8q,i} = |x_{r,8q,i} - x_c|, \quad i = 0, \ldots, 8q-1. \quad (11)$$

Following the work in [25], $\underline{\Delta}_{r,8q}$ is the magnitude component of the local difference. Similar to (9), $\underline{\Delta}_{r,8q}$ is transformed into

$$z_{r,q,i} = \frac{1}{q}\sum_{k=0}^{q-1} \Delta_{r,8q,(qi+k)}, \quad i = 0, \ldots, 7. \quad (12)$$

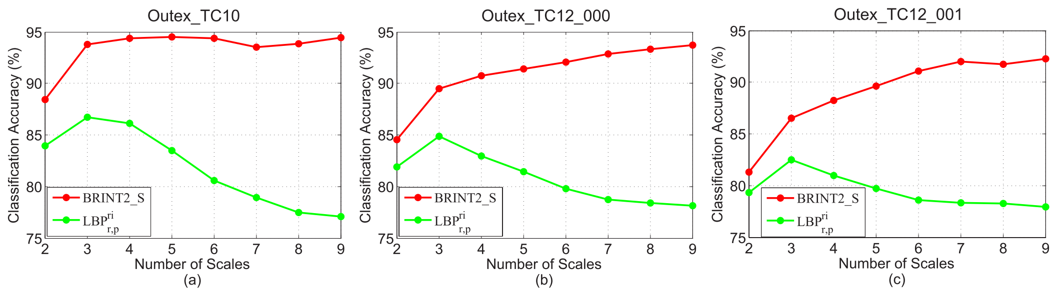

Fig. 5. Comparison of the classification accuracies of the proposed BRINT_S descriptor and the conventional LBP^{ri} descriptor, using all the three benchmark test suites from the Outex database designated by Ojala *et al.* [2]. (a) Results for Outex_TC10, (b) Results for Outex_TC12_000, and (c) Results for Outex_TC12_001. Sampling scheme 2 is used as defined in Fig. 4 (b). The experimental setup is kept consistent with those in [2]. The results firmly indicate that the proposed BRINT_S descriptor significantly outperforms the conventional LBP^{ri} descriptor.

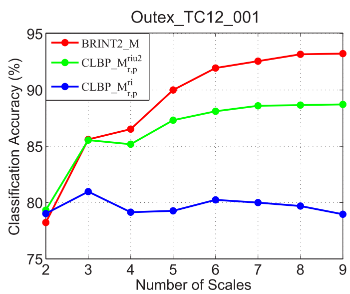

Fig. 6. Comparing the classification accuracies of the proposed BRINT_M with the corresponding CLBP results.

We compute a binary pattern BNT_M (Binary Noise Tolerant_Magnitude) based on $\underline{\underline{z}}$ via

$$\mathrm{BNT\_M}_{r,q} = \sum_{n=0}^{7} s(z_{r,q,n} - \mu_{r,q}^{l})2^n, \tag{13}$$

where μ_l is the local thresholding value. Note that the CLBP_M descriptor defined in [25, eq. (6)] uses the global threshold μ^g of (7), whereas in the original LBP operator the thresholding value is the center pixel value, which clearly varies from pixel to pixel. Therefore, instead of using a constant global threshold, we propose to use a locally varying one:

$$\mu_{r,q}^{l} = \frac{1}{8}\sum_{n=0}^{7} z_{r,q,n}. \tag{14}$$

With BNT_M defined, BRINT_M is defined as

$$\mathrm{BRINT\_M}_{r,q} = \min\{ROR(\mathrm{BNT\_M}_{r,q}, i) | i = 0, \ldots, 7\}. \tag{15}$$

Fig. 6 compares the results of the proposed BRINT_M with the comparable CLBP methods, with BRINT_M significantly outperforming.

Finally, consistent with CLBP, we also represent the center pixel in one of two bins:

$$\mathrm{BRINT\_C}_r = s(x_c - \mu_{I,r}) \tag{16}$$

where $\mu_{I,r}$ is the mean of the whole image excluding boundary pixels:

$$\mu_{I,r} = \frac{1}{(M-2r)(N-2r)} \sum_{i=r+1}^{M-r} \sum_{j=r+1}^{N-r} x(i,j). \tag{17}$$

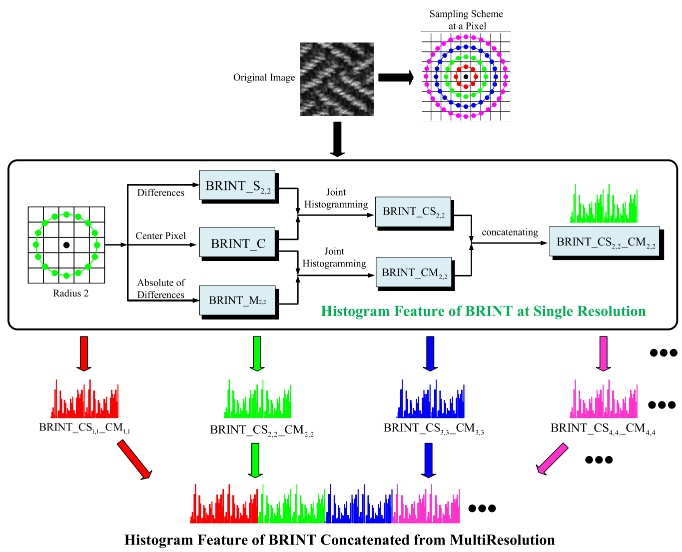

Fig. 7. The overall framework of the proposed multiresolution BRINT approach, whereby the BRINT_S, BRINT_M and BRINT_C histograms are concatenated over multiple scales.

C. Multi Resolution BRINT

The proposed BRINT descriptors were, so far, extracted from a single resolution with a circularly symmetric neighbor set of $8q$ pixels placed on a circle of radius r. Given that one goal of our approach is to cope with a large number of different scales, by altering r we can create operators for different spatial resolutions, ideally representing a textured patch by concatenating binary histograms from multiple resolutions into a single histogram, as illustrated in Fig. 7, clearly requiring that the histogram feature produced at each resolution be of low dimension.

Since BRINT_CSM, the joint histogram of BRINT_C, BRINT_S and BRINT_M, has a very high dimensionality of $36 * 36 * 2 = 2592$, in order to reduce the number of bins needed we adopt the $\mathrm{BRINT\_CS}_{r,q}\mathrm{\_CM}_{r,q}$ descriptor, meaning the joint histogram $\mathrm{BRINT\_C} * \mathrm{BRINT\_S}_{r,q}$ concatenated with $\mathrm{BRINT\_C} * \mathrm{BRINT\_M}_{r,q}$, producing a histogram of much lower dimensionality: $36 * 2 + 36 * 2 = 144$. As a point of comparison, in the experimental results we will also evaluate $\mathrm{BRINT\_S}_{r,q}\mathrm{\_M}_{r,q}$, having a dimensionality of $36 + 36 = 72$.

TABLE II

SUMMARY OF TEXTURE DATASETS USED IN OUR EXPERIMENTS

Experiment # 1

Texture Dataset	Image Rotation	Illumination Variation	Scale Variation	Texture Classes	Sample Size (pixels)	Samples per Class	Training Samples per Class	Test Samples per Class	Samples in Total
Outex_TC10	√			24	128 × 128	180	20	160	4320
Outex_TC12_000	√	√		24	128 × 128	200	20	180	4800
Outex_TC12_001	√	√		24	128 × 128	200	20	180	4800

Experiment # 2

Texture Dataset	Image Rotation	Illumination Variation	Scale Variation	Texture Classes	Sample Size (pixels)	Samples per Class	Training Samples per Class	Test Samples per Class	Samples in Total
CUReT	√	√		61	200 × 200	46	46	92	5612
Brodatz				24	64 × 64	25	13	12	600
KTH-TIPS2b	√	√	√	11	200 × 200	432	216	216	4752

D. Classification

The actual classification is performed via one of two popular classifiers:

1) The Nearest Neighbor Classifier (NNC) applied to the normalized BRINT histogram feature vectors $\underline{\boldsymbol{h}}_i$ and $\underline{\boldsymbol{h}}_j$, using the χ^2 distance metric as in [3], [5], [6], [25], and [38].
2) The nonlinear Support Vector Machine (SVM) of [43], where the benefits of SVMs for histogram-based classification have clearly been demonstrated in [4], [21], and [31]. Kernels commonly used include polynomials, Gaussian Radial Basis Functions and exponential Chi-Square kernel. Motivated by [4], [21], and [31], we focus on the exponential χ^2 kernel

$$K(\underline{\boldsymbol{h}}_i, \underline{\boldsymbol{h}}_j) = \exp(-\gamma\, \chi^2(\underline{\boldsymbol{h}}_i, \underline{\boldsymbol{h}}_j)), \tag{18}$$

where only one parameter γ needs to be optimized. We use the *one-against-one* technique, which trains a classifier for each possible pair of classes.

IV. EXPERIMENTAL EVALUATION

A. Image Data and Experimental Set up

For our experimental evaluation we have used six texture datasets, summarized in Table II, derived from the four most commonly used texture sources: the Brodatz album [32], the CUReT database [6] and KTHTIPS2b [42]. The Brodatz database is perhaps the best known benchmark for evaluating texture classification algorithms. Performing classification on the entire database is challenging due to the relatively large number of texture classes, the small number of examples for each class, and the lack of intra-class variation.

1) Experiment # 1: There are 24 different homogeneous texture classes selected from the Outex texture database [33], with each class having only one sample of size 538 × 746-pixels. The 24 different texture samples are imaged under different lighting and rotations conditions. Three experimental test suites **Outex_TC10**, **Outex_TC12_000** and **Outex_TC12_001**, summarized in Table II, were developed by Ojala *et al.* [2] as benchmark datasets for rotation and illumination invariant texture classification. For all the three test suites, the classifier is trained with 20 reference images of the 'inca' illumination condition and angle 0°, totaling 480 samples. The difference among these three test suites is in the testing set. For Outex_TC10, the remaining 3840 samples with 'inca' illumination, are used for testing the classifier. For Outex_TC12_000 and Outex_TC12_001, the classifier is tested with all 4320 images from fluorescent and sunlight lighting, respectively.

For the experiments on all three Outex databases, we first test the classification performance of the proposed approach on the original database and then assess the robustness of the proposed method under noisy conditions, where the original texture images are corrupted by zero-mean additive Gaussian noise with different Signal-to-Noise Ratios (SNRs) (defined as the ratio of signal power to the noise power). Moreover, we also test the classification performance of the proposed approach against impulse salt-and-pepper noise with different noise density ratio and multiplicative noise with zero mean and different variances, which is randomly and independently added to each image.

2) Experiment # 2: **Brodatz** was chosen to allow a direct comparison with the state-of-the-art results from [21]. There are 24 homogeneous texture classes.[2] Each image was partitioned into 25 nonoverlapping sub-images of size of 128×128, each of these downsampled to 64×64. 13 samples per class were selected randomly for training and the remaining 12 for testing.

For the **CUReT** database, we use the same subset of images which has been previously used in [3], [5], [6], [19], [25], [35], and [38]: 61 texture classes each with 92 images under varying illumination direction but at constant scale. 46 samples per class were selected randomly for training and the remaining 46 for testing. It has been argued [5], [6], [39] that this scale constancy is a major drawback of CUReT, leading to **KTHTIPS2b** [39], [42], with 3 viewing angles, 4 illuminants, and 9 different scales. We follow the training and testing scheme of [39]: training on three samples and testing on unseen samples.

For Brodatz and CUReT, results for texture classification under random Gaussian noisy environment are also provided. Training and testing scheme is the same as in noise-free situation.

B. Methods in Comparison and Implementation Details

We will be performing a comparative evaluation of our proposed approach, where the abbreviations of the proposed descriptor and state-of-the-art approaches are given in Table III:

1) **CLBP_CS**$^{ri}_{r,p}$**_CM**$^{ri}_{r,p}$: The rotation invariant CLBP approach parallel to our proposed BRINT_CS_CM feature.
2) **CLBP_CS**$^{riu2}_{r,p}$**_CM**$^{riu2}_{r,p}$: The rotation invariant and uniform CLBP method parallel to our proposed BRINT_CS_CM feature.
3) **DLBP+NGF** [21]: The fused features of the DLBP features and the normalized Gabor filter response average magnitudes (NGF). It is worth mentioning that the DLBP approach needs pretraining and the dimensionality of the DLBP feature varies with the training image.

[2]The 24 Brodatz textures are D1, D4, D16, D19, D21, D24, D28, D32, D53, D54, D57, D65, D68, D77, D82, D84, D92, D93, D95, D98, D101, D102, D106, D111

TABLE III
ABBREVIATION OF THE METHODS IN EXPERIMENTS AND THEIR CORRESPONDING MEANING

BRINT_S	Binary rotation invariant and noise tolerant descriptor based on sign component BRINT_$S_{r,q}$
BRINT_M	Binary rotation invariant and noise tolerant descriptor based on magnitude component BRINT_$M_{r,q}$
BRINT_C (CLBP_C)	Binary pattern for the center pixel
BRINT_S_M	Concatenation of BRINT_S and BRINT_M
BRINT_CS	Joint distribution of BRINT_C and BRINT_S
BRINT_CM	Joint distribution of BRINT_C and BRINT_M
BRINT_CS_CM	Concatenation of BRINT_CS and BRINT_CM
$\mathrm{LBP}^{ri}_{r,p}$(CLBP_$\mathrm{S}^{ri}_{r,p}$)	Rotation invariant LBP
$\mathrm{LTP}^{riu2}_{r,p}$	Rotation invariant uniform LTP
$\mathrm{LBP}^{riu2}_{r,p}$(CLBP_$\mathrm{S}^{riu2}_{r,p}$)	Rotation invariant uniform LBP
CLBP_$\mathrm{M}^{ri}_{r,p}$	Rotation invariant magnitude LBP
CLBP_$\mathrm{M}^{riu2}_{r,p}$	Rotation invariant uniform magnitude LBP
CLBP_$\mathrm{S}^{ri}_{r,p}$_$\mathrm{M}^{ri}_{r,p}$	Concatenation of CLBP_S^{ri} and CLBP_M^{ri}
CLBP_$\mathrm{S}^{riu2}_{r,p}$_$\mathrm{M}^{riu2}_{r,p}$	Concatenation of CLBP_$\mathrm{S}^{riu2}_{r,p}$ and CLBP_$\mathrm{M}^{riu2}_{r,p}$
CLBP_$\mathrm{CS}^{ri}_{r,p}$_$\mathrm{CM}^{ri}_{r,p}$	Concatenation of CLBP_$\mathrm{CS}^{riu2}_{r,p}$ and CLBP_$\mathrm{CM}^{riu2}_{r,p}$
CLBP_$\mathrm{CS}^{riu2}_{r,p}$_$\mathrm{CM}^{riu2}_{r,p}$	Concatenation of CLBP_$\mathrm{CS}^{riu2}_{r,p}$ and CLBP_$\mathrm{CM}^{riu2}_{r,p}$

TABLE IV
SAMPLING SCHEME, NOTATIONS AND COMPARISONS OF NUMBER OF BINS IN THE HISTOGRAM FEATURE FROM SINGLE SCALE (SS)

Method	Parameter	SS1	SS2	SS3	SS4	SS5	SS6	SS7	SS8	SS9
BRINT1_S	$(r, 8q)$	$(1,8)$	$(2,16)$	$(3,24)$	$(4,32)$	$(5,40)$	$(6,48)$	$(7,56)$	$(8,64)$	$(9,72)$
(BRINT1_M)	bins	36	36	36	36	36	36	36	36	36
BRINT2_S	$(r, 8q)$	$(1,8)$	$(2,24)$	$(3,24)$	$(4,24)$	$(5,24)$	$(6,24)$	$(7,24)$	$(8,24)$	$(9,24)$
(BRINT2_M)	bins	36	36	36	36	36	36	36	36	36
CLBP_$\mathrm{S}^{riu2}_{r,p}$	(r, p)	$(1,8)$	$(2,16)$	$(3,24)$	$(4,24)$	$(5,24)$	$(6,24)$	$(7,24)$	$(8,24)$	$(9,24)$
(CLBP_$\mathrm{M}^{riu2}_{r,p}$)	bins	10	18	26	26	26	26	26	26	26
$\mathrm{LTP}^{riu2}_{r,p}$	(r, p)	$(1,8)$	$(2,16)$	$(3,24)$	$(4,24)$	$(5,24)$	$(6,24)$	$(7,24)$	$(8,24)$	$(9,24)$
	bins	20	36	52	52	52	52	52	52	52
$\mathrm{NRLBP}^{riu2}_{r,p}$	(r, p)	$(1,8)$	$(2,8)$	$(3,8)$	$(4,8)$	$(5,8)$	$(6,8)$	$(7,8)$	$(8,8)$	$(9,8)$
	bins	10	10	10	10	10	10	10	10	10
CLBP_$\mathrm{S}^{ri}_{r,p}$	(r, p)	$(1,8)$	$(1,8)$	$(1,8)$	$(1,8)$	$(1,8)$	$(1,8)$	$(1,8)$	$(1,8)$	$(1,8)$
(CLBP_$\mathrm{M}^{ri}_{r,p}$)	bins	36	36	36	36	36	36	36	36	36

4) **LTP** [29]: The recommended $\mathbf{LTP}^{riu2}_{r,p}$ is used. Here we implemented a nine scale descriptor, where the associated parameter settings can be seen in Table IV.
5) **CLBP** [25]: The recommended fused descriptor CLBP_CSM (*i.e.* CLBP_$\mathrm{CS}^{riu2}_{r,p}\mathrm{M}^{riu2}_{r,p}$) is used, however only a 3-scale CLBP_CSM is implemented due to the high dimensionality limitation mentioned in Table I.
6) **LBP** [2]: The traditional rotation invariant uniform feature proposed by Ojala *et al.* [2]. We use a 3-scale descriptor as recommended by the authors.
7) **DNS+LBP** [19]: The fused feature of Dominant Neighborhood Structure approach and the conventional LBP approach proposed by Khellah [19] claimed to have noise robustness.
8) ***dis*CLBP** [15]: The discriminative descriptor obtained by a learning framework proposed by Guo *et al.* [15]. Due to the high dimensionality of the descriptor at larger scales, we use a 3-scale descriptor $dis(\mathrm{S{+}M})^{ri}_{r,p}$ as recommended by the authors.
9) $\mathbf{LBP}^{NT}_{r,p,k}$ [18]: A circular majority voting filter to achieve noise robustness, followed by a scheme to regroup the nonuniform LBP patterns into several different classes instead of classifying them into a single class as in $\mathrm{LBP}^{riu2}_{r,p}$. Parameter k acts as the size of kernel in the circular majority voting filter, controlling the number of noisy bits that should be filtered in the obtained LBP pattern. As suggested by Fathi *et al.* [18], parameter k is set as 1, 3 and 4 for p = 8, 16 and 24 respectively. We implemented a multiresolution (nine scales) $\mathrm{LBP}^{NT}_{r,p,k}$ (MS9),[3] however Fathi *et al.* [18] only considered three scales in their work.
10) **NRLBP** [20]: We implemented a multiresolution $\mathrm{NRLBP}^{riu2}_{r,p}$ descriptor: $\mathrm{NRLBP}^{riu2}_{r,8}, r = 1, \ldots, 9$, though Ren *et al.* [20] only evaluated the first scale $(r, p) = (1, 8)$ in their original paper. The reason that the number of neighboring points p is kept 8 for each radius r is because the extraction of the NRLBP feature requires building up a lookup table of size 3^p which is extremely expensive in terms of both computation time and memory cost.

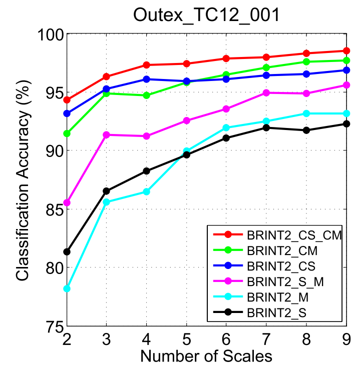

Fig. 8. Classification rates as a function of number of scales, with the same experimental setup as in Fig. 5, using a NNC classifier. Of the combinations tried, BRINT2_CS_CM performs the best.

Each texture sample is preprocessed: normalized to zero mean and unit standard deviation. For the CUReT and Brodatz databases, all results are reported over 100 random partitionings of training and testing sets. For SVM classification, we use the publicly available LibSVM library [41]. The parameters C and γ are searched exponentially in the ranges of $[2^{-5}, 2^{18}]$ and $[2^{-15}, 2^{8}]$, respectively, with a step size of 2^1 to probe the highest classification rate. However, in our experiments setting $C = 10^6$ and $\gamma = 0.01$ give very good performance. In the additive Gaussian noise environment, the SNRs tested here are 100, 30, 15, 10, 5 and 3, corresponding to 20db, 14.78db, 11.76db, 10db, 7db and 4.77db respectively. The noise density ratios of the salt-and-pepper noise tested are $\rho = 5\%, 10\%, 20\%, 30\%, 40\%$. The multiplicative noise tested is with zero mean and different variances $\upsilon = 0.02, 0.05, 0.1, 0.15, 0.2, 0.3$.

C. Results for Experiment # 1

Fig. 8 plots the classification performance of different BRINT combination schemes as a function of number of scales. There is a trend of increasing classification performance as the number of scales increases. It is apparent that the BRINT_CS_CM feature performs the best, therefore the BRINT_CS_CM descriptor will be our proposed choice and will be further evaluated.

Fig. 9 compares the two sampling schemes for the proposed approach, using the Outex_TC12_000 database. Here we can

[3] $\mathrm{LBP}^{NT}_{1,8,1}+\mathrm{LBP}^{NT}_{2,16,3}+\mathrm{LBP}^{NT}_{3,24,4}+\mathrm{LBP}^{NT}_{4,24,4}+\mathrm{LBP}^{NT}_{5,24,4}+\mathrm{LBP}^{NT}_{6,24,4}+\mathrm{LBP}^{NT}_{7,24,4}+\mathrm{LBP}^{NT}_{8,24,4}+\mathrm{LBP}^{NT}_{9,24,4}$.

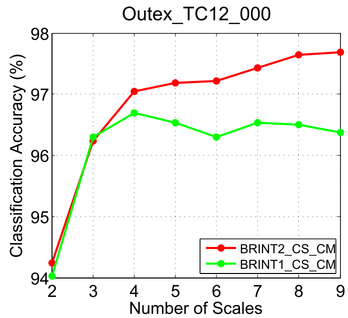

Fig. 9. Comparing the classification performance of the two sampling schemes of Fig. 4 on Outex_TC12_000. The experimental setup is the same as in Fig. 8. Scheme 2 performs better and will be adopted.

TABLE V

COMPARING THE CLASSIFICATION ACCURACIES (%) OF THE PROPOSED BRINT2_CS_CM DESCRIPTOR WITH TWO CONVENTIONAL CLBP DESCRIPTORS. ALL RESULTS ARE OBTAINED WITH A NNC CLASSIFIER. THE HIGHEST CLASSIFICATION ACCURACIES ARE HIGHLIGHTED IN BOLD FOR EACH TEST SUITE

Outex		Single Scale									Multiple Scales							
Databases	Methods	SS1	SS2	SS3	SS4	SS5	SS6	SS7	SS8	SS9	MS2	MS3	MS4	MS5	MS6	MS7	MS8	MS9
TC10	BRINT2_CS_CM	91.87	96.43	96.04	94.04	95.16	94.51	91.61	92.16	93.78	96.95	98.52	99.04	99.32	99.32	99.30	99.40	99.35
	CLBP_CS$^{ri}_{r,p}$_CM$^{ri}_{r,p}$	91.87	95.34	89.14	84.95	80.89	78.10	73.83	70.44	67.92	96.28	95.21	93.44	91.56	90.60	89.14	88.07	87.58
	CLBP_CS$^{riu2}_{r,p}$_CM$^{riu2}_{r,p}$	95.68	98.23	98.72	98.96	98.05	97.58	97.71	96.77	96.30	98.41	99.30	99.43	99.45	99.51	**99.53**	99.48	99.48
	LBP$^{NT}_{r,p,k}$ [18]	84.24	85.76	93.52	92.19	94.74	93.39	92.76	91.74	88.96	91.87	96.15	98.10	98.88	99.19	99.35	99.32	99.24
	NRLBP$^{riu2}_{r,p}$ [20]	89.79	89.24	88.31	84.35	77.01	77.81	77.01	65.41	62.16	93.78	96.67	97.01	98.07	97.81	95.60	95.05	93.44
TC12_000	BRINT2_CS_CM	86.46	93.38	94.47	91.06	92.15	89.86	89.65	89.38	90.72	94.24	96.23	97.04	97.18	97.22	97.43	97.64	**97.69**
	CLBP_CS$^{ri}_{r,p}$_CM$^{ri}_{r,p}$	86.46	92.62	88.56	81.27	79.86	77.62	73.36	69.63	67.94	93.17	94.56	93.29	91.25	88.82	87.55	86.92	86.41
	CLBP_CS$^{riu2}_{r,p}$_CM$^{riu2}_{r,p}$	89.81	94.31	94.88	93.98	90.56	87.85	88.26	88.29	87.71	95.63	96.81	96.67	96.23	95.95	96.00	96.00	95.97
	LBP$^{NT}_{r,p,k}$ [18]	69.70	80.42	85.42	86.57	85.95	84.47	82.99	85.05	82.18	84.72	91.46	94.05	94.42	95.19	96.00	96.34	96.18
	NRLBP$^{riu2}_{r,p}$ [20]	73.52	78.89	78.52	71.30	64.79	65.67	60.83	59.12	56.92	84.81	88.33	89.35	89.28	89.26	87.99	86.71	86.13
TC12_001	BRINT2_CS_CM	88.50	93.98	94.40	90.81	92.27	90.42	88.80	89.70	90.97	94.35	96.34	97.29	97.41	97.85	97.99	98.29	**98.56**
	CLBP_CS$^{ri}_{r,p}$_CM$^{ri}_{r,p}$	88.50	93.01	87.82	81.78	79.26	76.48	73.12	69.21	68.75	93.26	93.63	92.04	90.88	89.47	88.43	87.29	86.78
	CLBP_CS$^{riu2}_{r,p}$_CM$^{riu2}_{r,p}$	91.44	94.47	93.19	92.41	88.98	85.83	86.90	88.01	86.90	95.12	95.63	95.35	94.58	94.40	94.19	94.21	93.91
	LBP$^{NT}_{r,p,k}$ [18]	64.42	75.28	82.48	86.30	86.39	84.40	83.38	86.39	80.65	79.70	85.09	89.17	91.00	92.08	93.77	94.19	94.28
	NRLBP$^{riu2}_{r,p}$ [20]	69.19	73.36	79.19	72.99	67.69	69.14	60.53	58.33	57.48	81.18	85.76	88.50	89.86	91.13	89.58	88.24	87.38

see that sampling scheme 2 produced better classification performance than sampling scheme 1, believed to be because sampling scheme 1 oversmooths the local texture structure, resulting in lost texture information.

Table V compares the classification performance of the proposed BRINT2_CS_CM descriptor with those of CLBP [25] on the three Outex databases. We observe that BRINT2 performs significantly and consistently better than both *ri* and *riu2* forms of CLBP, both in single-scale and multiple-scale cases. The striking performance of BRINT2_CS_CM clearly demonstrates that the concatenated marginal distributions of the proposed basic BRINT_C, BRINT_S and BRINT_M codes and the novel "averaging before binarization" scheme turns out to be a very powerful representation of image texture. The use of multiple scales offers significant improvements over single-scale analysis, consistent with earlier results in Figs. 8 and 9, showing that the approach is making effective use of interactions between the center pixel and more distant pixels. To the best of our knowledge, the proposed approach produced classification scores which we believe to be the best reported for Outex_TC12_000 and Outex_TC12_001. Keeping in mind the variations in illumination and rotation present in the Outex databases, the results in Table V firmly demonstrate the illumination and rotation invariance property of the proposed BRINT_CS_CM approach.

Table VI compares the best classification scores achieved by the proposed BRINT2_CS_CM method using nine scales

TABLE VI

COMPARING THE CLASSIFICATION SCORES (%) ACHIEVED BY THE PROPOSED APPROACH WITH THOSE ACHIEVED BY RECENT STATE-OF-THE-ART TEXTURE CLASSIFICATION METHODS ON THE THREE OUTEX TEST SUITES IN EXPERIMENT # 1. SCORES ARE AS ORIGINALLY REPORTED, EXCEPT THOSE MARKED (◊) WHICH ARE TAKEN FROM THE WORK BY GUO *et al.* [25]

		Outex Database		
Classifier	Method	TC10	TC12_000	TC12_001
NNC	Ours: BRINT2_CS_CM (MS9)	**99.35**	97.69	**98.56**
SVM	Ours: BRINT2_CS_CM (MS9)	99.30	**98.13**	98.33
NNC	CLBP_CSM [25]	99.14	95.18	95.55
	CLBC_CSM [35]	98.96	95.37	94.72
	LBP$^{riu2}_{P,R}$/VAR$_{P,R}$ [2]	97.7	87.3	86.4
	LBPV$^{u2}_{P,R}$GM$^{P/2-1}_{PD2}$ [38]	97.63	95.06	93.88
	dis(S+M)$^{ri}_{r,p}$ [15]		97.0	96.5
	LBP$^{NT}_{r,p,k}$ [18] (MS9)	99.24	96.18	94.28
	NRLBP$^{riu2}_{r,p}$ (MS9) [20]	93.44	86.13	87.38
	VZ-MR8 [5]	93.59(◊)	92.55(◊)	92.82(◊)
	VZ-Patch [6]	92.00(◊)	91.41(◊)	92.06(◊)
SVM	DLBP+NGF [21]	99.1	93.2	90.4

(MS9) in comparison with state-of-the-art texture classification methods on all three Outex test suites. Despite not being customized to the separate test suites, our multi-scale BRINT2 descriptor produces what we believe to be the best reported results on all three suites, regardless whether NNC or SVM is used. We would also point out that except for the proposed BRINT, CLBP_CSM [25] and CLBC_CSM [35] approaches, the remaining descriptors listed in Table VI require an extra learning process to obtain the texton dictionary, requiring additional parameters or computational burden.

The preceding discussion allows us to assert that the proposed multi-scale BRINT2 approach outperforms the conventional multi-scale CLBP approach on the Outex test suites. We now wish to examine the robustness of our method against noise to test applicability to real-world applications, thus the original texture images from Experiment #1 have been subject to added Gaussian noise.

Table VII quite clearly shows the noise-robustness offered by the BRINT approach: similar classification rates are seen in the near-absence of noise (SNR=100), however the degree to which BRINT outperforms LBP [2], CLBP [25], LBP$^{NT}_{r,p,k}$ [18], $dis(\mathrm{S+M})^{ri}_{r,p}$ [15] and LTP$^{riu2}_{r,p}$ [29] becomes more and more striking as SNR is reduced, with classification rates more than 40% higher over all state-of-the-art methods in comparison at very low SNR.

Certainly the results in Table VII are consistent with the expected relative behavior of BRINT1 and BRINT2. The larger value of q in BRINT1, corresponding to greater pixel averaging, leads to poorer performance at high SNR, where excessive averaging is not desired, and persistently stronger performance at low SNR, where the averaging becomes an asset.

In addition to the result table shown in Table VII we also show the results of the statistical tests for significance we performed. The results are given in Table VIII, where the check sign indicates that a statistical significant difference between two results according to McNemar's test [37] was found. Clearly, it can be observed from Table VIII that the

TABLE VII

BRINT PERFORMANCE AS A FUNCTION OF NOISE, COMPARED WITH SEVERAL RECENT STATE-OF-THE-ART LBP VARIANTS. FOR EACH TEST GAUSSIAN NOISE WAS ADDED, AND THE HIGHEST CLASSIFICATION ACCURACY HIGHLIGHTED IN BOLD. THE NOISE ROBUSTNESS OF OUR PROPOSED BRINT IS QUITE STRIKING

Database	Features	Classification Accuracies (%)					
		SNR=100	SNR=30	SNR=15	SNR=10	SNR=5	SNR=3
Outex_TC10	BRINT1_CS_CM (MS9, NNC)	94.74	94.04	92.21	92.42	**89.24**	**77.50**
	BRINT2_CS_CM (MS9, NNC)	97.76	96.48	**95.47**	**92.97**	88.31	71.51
	CLBP_CS$_{r,p}^{riu2}$_CM$_{r,p}^{riu2}$ (MS9, NNC)	99.30	98.12	94.58	86.07	51.22	28.65
	LBP$_{r,p}^{riu2}$ (MS3, NNC) [2]	95.03	86.93	67.24	49.79	24.06	12.97
	LBP$_{r,p,k}^{NT}$ (MS9, NNC) [18]	98.65	96.12	88.85	80.23	51.09	30.34
	$dis(\mathrm{S}+\mathrm{M})_{r,p}^{ri}$ (NNC) [15]	96.07	82.60	56.72	39.66	19.66	8.83
	LTP$_{r,p}^{riu2}$ (MS9, NNC) [29]	**99.45**	**98.31**	93.44	84.32	57.37	27.73
	NRLBP$_{r,p}^{riu2}$ (MS9, NNC) [20]	87.40	85.73	80.16	72.42	51.02	32.63
Outex_TC12_000	BRINT1_CS_CM (MS9, NNC)	92.87	90.63	89.72	88.12	**83.84**	**74.47**
	BRINT2_CS_CM (MS9, NNC)	95.95	93.59	**91.32**	**90.49**	83.68	69.70
	CLBP_CS$_{r,p}^{riu2}$_CM$_{r,p}^{riu2}$ (MS9, NNC)	96.16	93.54	88.73	83.52	52.22	29.35
	LBP$_{r,p}^{riu2}$ (MS3, NNC) [2]	91.30	82.55	60.25	47.31	24.07	13.63
	LBP$_{r,p,k}^{NT}$ (MS9, NNC) [18]	92.15	89.35	83.77	74.47	49.84	31.27
	$dis(\mathrm{S}+\mathrm{M})_{r,p}^{ri}$ (NNC) [15]	91.55	78.06	54.98	37.36	18.24	8.77
	LTP$_{r,p}^{riu2}$ (MS9, NNC) [29]	**96.44**	**95.90**	89.42	82.27	53.06	27.89
	NRLBP$_{r,p}^{riu2}$ (MS9, NNC) [20]	84.49	81.16	77.52	70.16	50.88	33.31
Outex_TC12_001	BRINT1_CS_CM (MS9, NNC)	94.10	92.31	90.95	89.84	**85.83**	**76.04**
	BRINT2_CS_CM (MS9, NNC)	**96.92**	95.14	**93.66**	**92.29**	84.77	71.02
	CLBP_CS$_{r,p}^{riu2}$_CM$_{r,p}^{riu2}$ (MS9, NNC)	95.95	93.66	88.36	81.71	53.43	26.81
	LBP$_{r,p}^{riu2}$ (MS3, NNC) [2]	90.72	79.17	60.74	45.81	25.02	12.55
	LBP$_{r,p,k}^{NT}$ (MS9, NNC) [18]	94.35	90.81	84.95	75.49	47.04	30.38
	$dis(\mathrm{S}+\mathrm{M})_{r,p}^{ri}$ (NNC) [15]	92.92	79.63	54.93	37.43	18.06	9.12
	LTP$_{r,p}^{riu2}$ (MS9, NNC) [29]	96.74	**95.76**	89.63	81.50	53.45	26.37
	NRLBP$_{r,p}^{riu2}$ (MS9, NNC) [20]	85.76	82.69	77.38	69.68	49.07	32.06

TABLE VIII

RESULTS OF MCNEMAR'S TEST FOR STATISTICAL SIGNIFICANCE ANALYSIS (AT A SIGNIFICANCE LEVEL OF 0.025) BETWEEN THE RESULTS OF THE PROPOSED BRINT AND THOSE BY THE STATE-OF-THE-ART METHODS ON THE OUTEX_TC12_000 TEST SUITE INJECTED WITH ADDITIVE GAUSSIAN NOISE (CORRESPONDING TO THE RESULTS ON THE OUTEX_TC12_000 SHOWN IN TABLE VII). THE $\surd$ MARK INDICATES STATISTICALLY SIGNIFICANCE EXISTENCE. THE BRACKETED VALUES ARE THE MCNEMAR CHI-SQUARE STATISTICS AND THE p VALUES ($a = 0.000$, $b = 0.004$)

Features	BRINT2_CS_CM (MS9) (Proposed)					
	SNR=100	SNR=30	SNR=15	SNR=10	SNR=5	SNR=3
CLBP_CS$_{r,p}^{riu2}$_CM$_{r,p}^{riu2}$ (MS9)	$\surd(35.7, p=a)$	$\surd(25.3, p=a)$	$\surd(48.7, p=a)$	$\surd(157.6, p=a)$	$\surd(562.0, p=a)$	$\surd$ (303.9, $p=a$))
LBP$_{r,p}^{riu2}$ (MS3)	$\surd(216.0, p=a)$	$\surd(405.6, p=a)$	$\surd(864.0, p=a)$	$\surd(1163.1, p=a)$	$\surd(1277.5, p=a)$	$\surd$ (455.8, $p=a$))
LBP$_{r,p,k}^{NT}$ (MS9)	$\surd(66.4, p=a)$	$\surd(36.2, p=a)$	$\surd(75.5, p=a)$	$\surd(335.1, p=a)$	$\surd(534.3, p=a)$	$\surd$ (262.0, $p=a$))
$dis(\mathrm{S}+\mathrm{M})_{r,p}^{ri}$ (MS3)	$\surd(161.6, p=a)$	$\surd(677.6, p=a)$	$\surd(1077.1, p=a)$	$\surd(1539.1, p=a)$	$\surd(1491.2, p=a)$	$\surd$ (589.2, $p=a$))
LTP$_{r,p}^{riu2}$ (MS9)	$\surd(40.5, p=a)$	$\surd(8.2, p=b)$	$\surd(117.8, p=a)$	$\surd(222.7, p=a)$	$\surd(496.1, p=a)$	$\surd$ (288.5, $p=a$))
NRLBP$_{r,p}^{riu2}$ (MS9)	$\surd(232.9, p=a)$	$\surd(205.5, p=a)$	$\surd(201.2, p=a)$	$\surd(356.6, p=a)$	$\surd(550.7, p=a)$	$\surd$ (248.4, $p=a$)

differences between the proposed BRINT approach and the state-of-the-art results are all statistically significant.

Fig. 10 plots the classification results as a function of scale, contrasting the classification behaviors of the proposed BRINT2 and conventional CLBP descriptors under high noise (SNR=5). The strength of using multiple scales rather than a single scale is clearly seen, as is the significant performance improvement of BRINT2 over CLBP.

Finally, Table IX and Table X compare the classification performance of our proposed BRINT2_CS_CM descriptor with several recent state-of-the-art methods in the presence of salt-and-pepper noise and multiplicative noise respectively. It is observed from Table IX and Table X that our proposed BRINT2 approach performs consistently better than all state-of-the-art methods. As the noise level increases, the performance gain of the proposed approaches over other approaches in comparison becomes more significant, clearly demonstrating the robustness of BRINT to both impulsive noise and multiplicative noise.

TABLE IX

BRINT PERFORMANCE AS A FUNCTION OF NOISE DENSITY RATIO (ρ), COMPARED WITH SEVERAL RECENT STATE-OF-THE-ART LBP VARIANTS. THE OUTEX_TC12_001 TEST SUITE IS USED FOR EXPERIMENTS. FOR EACH TEST SALT-AND-PEPPER NOISE WITH DIFFERENT NOISE DENSITY RATIO (ρ) WAS ADDED, AND THE HIGHEST CLASSIFICATION ACCURACY HIGHLIGHTED IN BOLD. THE NNC CLASSIFIER IS USED

Features	Classification Accuracies (%)				
	$\rho = 5\%$	$\rho = 10\%$	$\rho = 20\%$	$\rho = 30\%$	$\rho = 40\%$
BRINT2_CS_CM (MS9)	**98.63**	**96.55**	**92.64**	**84.54**	**74.26**
CLBP_CS$_{r,p}^{riu2}$_CM$_{r,p}^{riu2}$ (MS9)	92.96	90.53	82.20	69.77	50.88
$dis(\mathrm{S}+\mathrm{M})_{r,p}^{ri}$ [15]	94.77	93.22	76.67	54.81	43.33
LTP$_{r,p}^{riu2}$ (MS9) [29]	92.89	91.99	86.11	77.71	64.19
NRLBP$_{r,p}^{riu2}$ (MS9) [20]	88.63	88.96	83.87	78.98	67.11

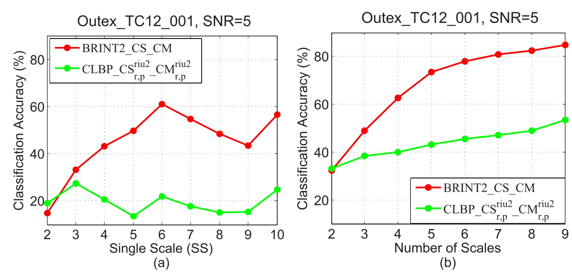

Fig. 10. A comparison of classification performance under severe noise (SNR = 5), both (a) as a function of the single scale used, and (b) as a function of the *number* of scales. The strength of BRINT2 over CLBP is clear, as is the benefit of forming features over as many scales as possible.

TABLE X

COMPARING THE PERFORMANCE OF DIFFERENT DESCRIPTORS ON THE OUTEX_TC12_001 TEST SUITE INJECTED WITH MULTIPLICATIVE NOISE. FOR EACH TEST MULTIPLICATIVE NOISE WITH ZERO MEAN AND VARIANCE v WAS ADDED, AND THE HIGHEST CLASSIFICATION ACCURACY HIGHLIGHTED IN BOLD. THE NNC CLASSIFIER IS USED

Features	Classification Accuracies (%)					
	$v = 0.02$	$v = 0.05$	$v = 0.1$	$v = 0.15$	$v = 0.2$	$v = 0.3$
BRINT2_CS_CM (MS9)	95.90	**93.31**	**90.76**	**88.06**	**85.95**	**72.82**
CLBP_CS$_{r,p}^{riu2}$_CM$_{r,p}^{riu2}$ (MS9)	93.31	90.44	83.77	72.06	63.56	47.43
$dis(\mathrm{S}+\mathrm{M})_{r,p}^{ri}$ [15]	89.98	76.39	49.72	39.40	29.26	22.99
LTP$_{r,p}^{riu2}$ (MS9) [29]	**95.97**	92.08	82.85	72.50	61.39	47.25
NRLBP$_{r,p}^{riu2}$ (MS9) [20]	84.03	80.56	72.08	65.88	56.46	47.25

D. Results for Experiment # 2

The classification results on the original Brodatz databases are listed in Table XI. The proposed BRINT1 method with a NNC classifier performs the best at 100% accuracy, however honestly all of the tested methods achieve very high classification accuracies here, since all 24 tested textures are relatively homogeneous and have small intra-class variations caused by rotation and illumination variations, a relatively easy problem for classification.

Instead, the noise-corrupted Brodatz database is expected to introduce greater challenges, with results listed in Table XII.

TABLE XI

COMPARING THE CLASSIFICATION ACCURACIES (%) OF THE PROPOSED BRINT_CS_CM WITH THE CONVENTIONAL CLBP_CS$^{riu2}_{r,p}$_CM$^{riu2}_{r,p}$ AND TWO STATE-OF-THE-ART APPROACHES ON THE ORIGINAL BRODATZ DATABASE. ALL OUR RESULTS ARE REPORTED OVER 100 RANDOM PARTITIONINGS OF THE TRAINING AND TEST SET. THE HIGHEST CLASSIFICATION SCORE IS HIGHLIGHTED IN BOLD

	Multiple Scale							
Methods	MS2	MS3	MS4	MS5	MS6	MS7	MS8	MS9
BRINT1_CS_CM (SVM)	99.72 ± 0.42	99.78 ± 0.32	99.76 ± 0.30	99.78 ± 0.29	99.67 ± 0.32	99.54 ± 0.34	99.44 ± 0.39	99.37 ± 0.44
BRINT1_CS_CM (NNC)	99.85 ± 0.22	**100.00 ± 0.00**	99.98 ± 0.09	99.88 ± 0.21	99.79 ± 0.25	99.59 ± 0.34	99.39 ± 0.41	99.22 ± 0.49
BRINT2_CS_CM (SVM)	99.88 ± 0.28	99.93 ± 0.14	99.93 ± 0.16	99.82 ± 0.25	99.74 ± 0.35	99.67 ± 0.29	99.46 ± 0.37	99.31 ± 0.45
BRINT2_CS_CM (NNC)	99.66 ± 0.47	99.81 ± 0.34	99.85 ± 0.23	99.77 ± 0.28	99.69 ± 0.32	99.69 ± 0.31	99.54 ± 0.39	99.45 ± 0.44
CLBP_CS$^{riu2}_{r,p}$_CM$^{riu2}_{r,p}$ (NNC)	99.70 ± 0.44	99.72 ± 0.33	99.81 ± 0.31	99.68 ± 0.24	99.59 ± 0.35	99.59 ± 0.36	99.35 ± 0.38	99.29 ± 0.43
DLBP+NGF [21] (SVM)	99.16 (DLBP$_{r=3}$+NGF)				99.54 (DLBP$_{r=2}$+NGF)			
LBP [2] (NNC)	98.48 ± 0.52							

TABLE XII

A COMPARISON OF CLASSIFICATION ACCURACY (%) ON THE BRODATZ24 DATASET WITH ADDITIVE GAUSSIAN NOISE. FOR EACH NOISE LEVEL THE TWO HIGHEST MEAN CLASSIFICATION ACCURACIES ARE HIGHLIGHTED IN BOLD. RESULTS ARE REPORTED OVER 100 RANDOM PARTITIONINGS OF THE TRAINING AND TEST SETS. THE SVM CLASSIFIER IS USED

	Classification Accuracies (%)					
Features	SNR=100	SNR=30	SNR=15	SNR=10	SNR=5	SNR=3
BRINT1_CS_CM (MS7)	**99.00 ± 0.46**	**98.09 ± 0.78**	**96.60 ± 0.76**	**95.47 ± 0.90**	**91.27 ± 1.44**	**84.15 ± 1.63**
BRINT1_CS_CM (MS9)	98.60 ± 0.48	97.81 ± 0.59	96.42 ± 0.88	**95.36 ± 0.96**	**91.00 ± 1.41**	**85.56 ± 1.62**
BRINT2_CS_CM (MS7)	98.95 ± 0.60	98.07 ± 0.65	**96.84 ± 0.89**	94.94 ± 1.36	89.59 ± 1.19	81.67 ± 1.80
BRINT2_CS_CM (MS9)	98.60 ± 0.52	97.68 ± 0.68	96.55 ± 0.89	94.50 ± 1.37	89.65 ± 1.27	82.31 ± 1.69
CLBP_CS$^{riu2}_{r,p}$_CM$^{riu2}_{r,p}$ (MS7)	98.94 ± 0.62	97.05 ± 0.75	94.53 ± 1.12	91.16 ± 1.43	82.50 ± 1.78	72.02 ± 2.10
CLBP_CS$^{riu2}_{r,p}$_CM$^{riu2}_{r,p}$ (MS9)	98.68 ± 0.71	97.17 ± 0.86	94.65 ± 1.10	91.10 ± 1.47	83.39 ± 1.85	73.10 ± 2.19
DLBP$_2$+NGF [21]	**99.35 ± 0.00**	**99.31 ± 0.00**	95.77 ± 0.00	92.33 ± 4.65	83.84 ± 4.48	NA
LBP$^{riu2}_{r,p}$ (MS3) [2]	96.88 ± 0.82	91.56 ± 1.42	85.24 ± 1.79	80.56 ± 2.15	65.79 ± 1.92	50.40 ± 2.22

TABLE XIII

COMPARING THE CLASSIFICATION SCORES (%) ACHIEVED BY THE PROPOSED APPROACH WITH THOSE ACHIEVED BY RECENT STATE-OF-THE-ART METHODS ON THE CURET DATABASE. SCORES ARE AS ORIGINALLY REPORTED, EXCEPT THAT MARKED (∗) WHICH WAS TAKEN FROM [4]

		CUReT	Published in
NNC	BRINT2_S_M (MS9)	97.86	This paper
	BRINT2_CS_CM (MS9)	97.06	This paper
SVM	BRINT2_S_M (MS9)	99.19	This paper
	BRINT2_CS_CM (MS9)	**99.27**	This paper
NNC	CLBP_CSM [25]	97.39	TIP 2010
	CLBC_CSM [35]	95.39	TIP 2012
	LBPV$^{u2}_{P,R}$GM$^{p/2-1}_{PD2}$ [38]	96.04	PR 2010
	dis(S+M)$^{ri}_{r,p}$ [15]	98.3	PR 2012
	DNS + LBP$_{24,3}$ [19]	94.52	TIP 2011
	VZ-MR8 [5]	97.43	IJCV 2005
	VZ-Patch [6]	98.03	TPAMI 2009
	Lazebnik *et al.* [10]	72.5(∗)	TPAMI 2005
	MultiScale BIF [7]	98.6	IJCV 2010
	RP [3]	98.52	TPAMI 2012
SVM	Hayman *et al.* [31]	98.46	IMAVIS 2010
	Zhang *et al.* [4]	95.3	IJCV 2007
	LBP$^{NT}_{r,p,k}$ (MS9, SVM) [18]	98.07	PRL 2012

TABLE XIV

CLASSIFICATION ACCURACIES (%) ON THE NOISE-CORRUPTED CURET DATABASE. FOR EACH TEST, THE FOUR HIGHEST MEAN CLASSIFICATION ACCURACIES ARE HIGHLIGHTED IN BOLD. ALL RESULTS ARE REPORTED OVER 100 RANDOM PARTITIONINGS OF THE TRAINING AND TEST SETS

	Classification Accuracies (%)					
Features	SNR=100	SNR=30	SNR=15	SNR=10	SNR=5	SNR=3
BRINT1_CS_CM (MS7, SVM)	**98.61 ± 0.66**	**97.20 ± 0.95**	**95.98 ± 0.67**	**94.05 ± 0.67**	**89.90 ± 1.24**	**85.86 ± 1.84**
BRINT1_CS_CM (MS9, SVM)	**98.65 ± 0.66**	**97.52 ± 0.60**	**96.26 ± 0.86**	**94.68 ± 1.00**	**90.65 ± 1.28**	**86.47 ± 1.70**
BRINT1_CS_CM (MS7, NNC)	96.67 ± 0.75	94.76 ± 0.83	92.86 ± 1.03	90.00 ± 2.56	85.02 ± 1.24	78.54 ± 0.99
BRINT1_CS_CM (MS9, NNC)	96.81 ± 0.72	95.39 ± 0.84	93.69 ± 1.09	90.92 ± 2.55	86.11 ± 1.17	80.45 ± 1.05
BRINT2_CS_CM (MS7, SVM)	**98.70 ± 0.43**	**97.28 ± 0.73**	**95.07 ± 0.84**	**93.90 ± 0.87**	**89.26 ± 1.23**	**84.49 ± 1.54**
BRINT2_CS_CM (MS9, SVM)	**98.75 ± 0.53**	**97.32 ± 0.63**	**95.70 ± 0.96**	**94.07 ± 1.20**	**90.00 ± 1.23**	**84.98 ± 1.84**
BRINT2_CS_CM (MS7, NNC)	96.57 ± 0.71	94.48 ± 0.96	92.31 ± 0.89	89.99 ± 1.12	83.35 ± 1.19	77.04 ± 1.24
BRINT2_CS_CM (MS9, NNC)	96.78 ± 0.71	94.90 ± 0.71	92.83 ± 0.87	90.46 ± 1.11	84.48 ± 1.27	78.33 ± 1.26
CLBP_CS$^{riu2}_{r,p}$_CM$^{riu2}_{r,p}$ (MS7, SVM)	98.24 ± 0.78	95.92 ± 0.92	92.65 ± 0.84	90.16 ± 0.86	82.27 ± 1.25	74.77 ± 1.54
CLBP_CS$^{riu2}_{r,p}$_CM$^{riu2}_{r,p}$ (MS9, SVM)	98.40 ± 0.47	95.75 ± 2.25	92.82 ± 1.00	90.58 ± 1.14	83.13 ± 1.32	75.42 ± 1.41
CLBP_CS$^{riu2}_{r,p}$_CM$^{riu2}_{r,p}$ (MS7, NNC)	95.05 ± 0.82	90.89 ± 1.20	86.51 ± 0.99	81.66 ± 1.24	73.34 ± 1.45	64.18 ± 1.23
CLBP_CS$^{riu2}_{r,p}$_CM$^{riu2}_{r,p}$ (MS9, NNC)	95.19 ± 0.86	91.12 ± 1.22	86.58 ± 1.04	82.35 ± 1.18	73.55 ± 1.45	64.77 ± 1.26
DNS+LBP$_{24,3}$ [19] (NNC)	91.57 ± 1.18	87.37 ± 0.76	83.28 ± 1.20	81.04 ± 1.19	72.71 ± 0.97	NA
LBP$^{riu2}_{r,p}$ (SVM) [2]	92.54 ± 0.99	87.18 ± 0.99	81.23 ± 1.24	77.10 ± 1.18	67.14 ± 1.65	58.20 ± 1.41
LBP$^{NT}_{r,p,k}$ (MS9, NNC) [18]	91.56 ± 1.56	85.99 ± 1.09	78.98 ± 1.25	74.90 ± 0.91	65.74 ± 0.88	56.31 ± 1.11
LBP$^{NT}_{r,p,k}$ (MS9, SVM) [18]	95.14 ± 0.91	89.12 ± 0.97	85.68 ± 1.78	82.43 ± 1.16	72.70 ± 1.58	63.61 ± 1.26
LTP$^{riu2}_{r,p}$ (MS9, NNC) [29]	92.22 ± 1.28	90.15 ± 1.38	86.66 ± 1.26	84.85 ± 0.91	77.48 ± 1.67	70.67 ± 1.90
LTP$^{riu2}_{r,p}$ (MS9, SVM) [29]	98.05 ± 0.83	95.99 ± 0.56	93.38 ± 1.54	91.24 ± 1.51	86.50 ± 1.01	79.00 ± 1.39

We specifically compare with DLBP+NGF [21], which is one of the few LBP-based approach to claim noise robustness. Certainly DLBP+NGF significantly outperforms LBP$^{riu2}_{r,p}$ [2], and slightly better than CLBP_CS$^{riu2}_{r,p}$_CM$^{riu2}_{r,p}$, however in cases of higher noise (lower SNR) the proposed BRINT approaches significantly outperform both CLBP and DLBP+NGF.

The CUReT database contains 61 texture classes with each class having 92 samples imaged under different viewpoints and illuminations, a greater classification challenge than Brodatz. Table XIII compares performance with the state of the art, where the proposed BRINT2 with nine scales using SVM produces the highest classification score.

Table XIV tests classification robustness to noise. The results firmly demonstrate the noise tolerant performance of the proposed methods. To the best of our knowledge, the DNS+LBP$_{24,3}$ [19] is the only LBP related method which claims noise tolerance and has reported CUReT results. Our proposed methods consistently and significantly outperform LBP, CLBP, DNS+LBP [19] and LBP$^{NT}_{r,p,k}$ [18], with the relative performance difference increasing as the noise level increases.

Although the DNS+LBP$_{24,3}$ [19] approach sacrifices some performance in classifying noise-free textures for the sake of obtaining noise robustness, this is not the case for our proposed approach. Fig. 11 shows classification performance on the KTHTIPS2b database, demonstrating that our proposed approach outperforms comparative state of the art, while simultaneously maintaining noise robustness.

Finally, Table XV illustrates the effect of introducing a Gaussian pre-smoothing filter, showing results with and without pre-smoothing. We observe that the proposed BRINT2 is only very modestly improved, if at all, by pre-smoothing, due to the noise robustness inherent in the method. We also observe that LBP$^{NT}_{r,p,k}$ [18] performs poorly, regardless of

TABLE XV

CLASSIFICATION ACCURACIES (%) ON THE NOISE-CORRUPTED CUReT DATABASE, COMPARING THE METHODS WITH OR WITHOUT PRE-GAUSSIAN SMOOTHING. ALL RESULTS ARE REPORTED OVER 50 RANDOM PARTITIONINGS OF THE TRAINING AND TEST SETS. FOR EACH TEST, THE HIGHEST MEAN CLASSIFICATION ACCURACIES ARE HIGHLIGHTED IN BOLD. FOR GAUSSIAN SMOOTHING FILTER, A 7×7 FILTER MATRIX WITH $\sigma = 1.5$ IS USED. FOR CLASSIFICATION, THE SVM CLASSIFIER IS USED

Features	Classification Accuracies (%)					
	SNR=100	SNR=30	SNR=15	SNR=10	SNR=5	SNR=3
BRINT2_CS_CM (MS9)	**98.75 ± 0.53**	97.32 ± 0.63	95.70 ± 0.96	94.07 ± 1.20	90.00 ± 1.23	84.98 ± 1.84
Gaussian+BRINT2_CS_CM (MS9)	98.33 ± 0.66	**97.84 ± 0.33**	**96.82 ± 0.75**	**94.73 ± 0.92**	91.59 ± 1.19	87.52 ± 1.82
CLBP_CS$^{riu2}_{r,p}$_CM$^{riu2}_{r,p}$ (MS9)	98.40 ± 0.47	95.75 ± 2.25	92.82 ± 1.00	90.58 ± 1.14	83.13 ± 1.32	75.42 ± 1.41
Gaussian+CLBP_CS$^{riu2}_{r,p}$_CM$^{riu2}_{r,p}$ (MS9)	98.21 ± 0.44	97.61 ± 0.55	96.48 ± 0.86	94.55 ± 0.56	**91.80 ± 0.83**	**87.80 ± 0.96**
LBP$^{NT}_{r,p,k}$ (MS9) [18]	95.14 ± 0.91	89.12 ± 0.97	85.68 ± 1.78	82.43 ± 1.16	72.70 ± 1.58	63.61 ± 1.26
Gaussian+LBP$^{NT}_{r,p,k}$ (MS9) [18]	92.88 ± 1.35	90.05 ± 0.93	87.00 ± 1.77	82.94 ± 1.02	76.50 ± 1.67	69.95 ± 1.35
LTP$^{riu2}_{r,p}$ (MS9) [29]	98.05 ± 0.83	95.99 ± 0.56	93.38 ± 1.54	91.24 ± 1.51	86.50 ± 1.01	79.00 ± 1.39
Gaussian+LTP$^{riu2}_{r,p}$ (MS9) [29]	97.55 ± 0.83	96.52 ± 0.94	95.88 ± 1.16	93.68 ± 0.76	89.04 ± 1.47	84.68 ± 0.97

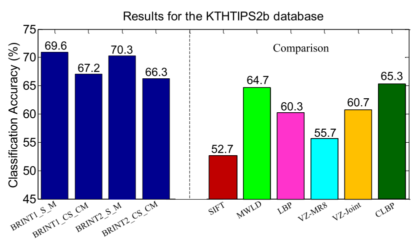

Fig. 11. Classification performance of the proposed approach with various state-of-the-art results on the KTHTIPS2b texture material database. The BRINT results are based on nine scales and NNC. All results are computed by us, except for those of MWLD and SIFT, which are quoted from [40].

SNR or filtering, whereas the proposed BRINT2 gives the highest performance at high SNR, and at lower SNR only a modest difference is present between BRINT2 and the Gaussian+CLBP_CS$^{riu2}_{r,p}$_CM$^{riu2}_{r,p}$ method.

Results in Table XV confirm the noise robustness of the proposed BRINT approach, emphasizing that no smoothing is necessary. The absence of spatial smoothing is a significant advantage for BRINT, as local spatial information is important for texture classification, whereas pre-smoothing can suppress important local texture information, a serious drawback for texture recognition in low-noise situations.

V. CONCLUSIONS

The multi-resolution LBP$^{riu2}_{r,p}$ and the more recent CLBP_CS$^{riu2}_{r,p}$M$^{riu2}_{r,p}$ descriptors have been proved to be two powerful measures of image texture [2], [25]. However, they have also been shown to have serious limitations including the instability of the uniform patterns, the lack of noise robustness, the inability to encode a large number of different local neighborhoods, an incapability to cope with large local neighborhoods, and high dimensionality (CLBP) [13], [21], [23]. In order to avoid these problems, we have presented BRINT, a theoretically and computationally simple, noise tolerant yet highly effective multi-resolution descriptor for rotation invariant texture classification. The proposed BRINT descriptor is shown to exhibit very good performance on popular benchmark texture databases under both normal conditions and noise conditions.

The main contributions of this work include the development of a novel and simple strategy — circular averaging before binarization — to compute a local binary descriptor based on the conventional LBP approach. The proposed approach firmly puts rotation invariant binary patterns back on the map, after they were shown to be very ineffective in [2] and [34]. Since the key advantage of the traditional LBP approach has been its computational simplicity, in our opinion a complicated or computationally expensive LBP variant violates the whole premise of the LBP idea. Our proposed BRINT is firmly consistent with the goal of simplicity and efficiency.

The proposed BRINT descriptor is noise robust, in contrast to the noise sensitivity of the traditional LBP and its many variants. Furthermore the proposed idea can be generalized and integrated with existing LBP variants, such as conventional LBP, rotation invariant patterns, rotation invariant uniform patterns, CLBP, Local Ternary Patterns (LTP) and $dis(\mathrm{S}+\mathrm{M})^{ri}_{r,p}$ to derive new image features for texture classification.

The robustness of the proposed approach to image rotation and noise has been validated with extensive experiments on *six* different texture datasets. This noise robustness characteristic is evaluated quantitatively with different artificially generated types and levels of noise (including Gaussian, salt and pepper and multiplicative noise) in natural texture images. The proposed approach to produce consistently good classification results on all of the datasets, most significantly outperforming the state-of-the-art methods in high noise conditions.

The current work has focused on texture classification. Future interest lies how to exploit the proposed descriptor for the domain of face recognition and object recognition.

REFERENCES

[1] X. Xie and M. Mirmehdi, "A galaxy of texture features," in *Handbook of Texture Analysis*, M. Mirmehdi, X. Xie, J. Suri, Eds. London, U.K.: Imperial College Press, 2008, pp. 375–406.

[2] T. Ojala, M. Pietikäinen, and T. Mäenpää, "Multiresolution gray-scale and rotation invariant texture classification with local binary patterns," *IEEE Trans. Pattern Anal. Mach. Intell.*, vol. 24, no. 7, pp. 971–987, Jul. 2002.

[3] L. Liu and P. Fieguth, "Texture classification from random features," *IEEE Trans. Pattern Anal. Mach. Intell.*, vol. 34, no. 3, pp. 574–586, Mar. 2012.

[4] J. Zhang, M. Marszalek, S. Lazebnik, and C. Schmid, "Local features and kernels for classification of texture and object categories: A comprehensive study," *Int. J. Comput. Vis.*, vol. 73, no. 2, pp. 213–238, 2007.

[5] M. Varma and A. Zisserman, "A statistical approach to texture classification from single images," *Int. J. Comput. Vis.*, vol. 62, nos. 1–2, pp. 61–81, 2005.

[6] M. Varma and A. Zisserman, "A statistical approach to material classification using image patches," *IEEE Trans. Pattern Anal. Mach. Intell.*, vol. 31, no. 11, pp. 2032–2047, Nov. 2009.

[7] M. Crosier and L. D. Griffin, "Using basic image features for texture classification," *Int. J. Comput. Vis.*, vol. 88, no. 3, pp. 447–460, 2010.

[8] B. S. Manjunathi and W. Y. Ma, "Texture features for browsing and retrieval of image data," *IEEE Trans. Pattern Anal. Mach. Intell.*, vol. 18, no. 8, pp. 837–842, Aug. 1996.

[9] L. Liu, B. Yang, P. Fieguth, Z. Yang, and Y. Wei, "BRINT: A binary rotation invariant and noise tolerant texture descriptor," in *Proc. IEEE ICIP*, Sep. 2013, pp. 255–259.

[10] S. Lazebnik, C. Schmid, and J. Ponce, "A sparse texture representation using local affine regions," *IEEE Trans. Pattern Anal. Mach. Intell.*, vol. 27, no. 8, pp. 1265–1278, Aug. 2005.

[11] T. Ojala, M. Pietikäinen, and D. Harwood, "A comparative study of texture measures with classification based on feature distributions," *Pattern Recognit.*, vol. 29, no. 1, pp. 51–59, 1996.

[12] A. Fernández, M. Álvarez, and F. Bianconi, "Texture description through histograms of equivalent patterns," *J. Math. Imag. Vis.*, vol. 45, no. 1, pp. 76–102, Jan. 2013.

[13] D. Huang, C. Shan, M. Ardabilian, Y. Wang, and L. Chen, "Local binary patterns and its application to facial image analysis: A survey," *IEEE Trans. Syst., Man, Cybern. C, Appl. Rev.*, vol. 41, no. 6, pp. 765–781, Nov. 2011.

[14] M. Heikkilä, M. Pietikänen, and C. Schmid, "Description of interest regions with local binary patterns," *Pattern Recognit.*, vol. 42, no. 3, pp. 425–436, 2009.

[15] Y. Guo, G. Zhao, and M. Pietikäinen, "Discriminative features for texture description," *Pattern Recgnit.*, vol. 45, pp. 3834–3843, 2012.

[16] M. Teutsch and J. Beyerer, "Noise resistant gradient calculation and edge detection using local binary patterns," in *Proc. Asian Conf. Comput. Vis. Workshop*, 2013, pp. 1–14.

[17] M. Paci, L. Nanni, A. Lahti, K. Aalto-Setälä, J. Hyttinen, and S. Severi, "Non-binary coding for texture descriptors in sub-cellular and stem cell image classification," *Current Bioinformat.*, vol. 8, no. 2, pp. 208–219, 2013.

[18] A. Fathi and A. R. Naghsh-Nilchi, "Noise tolerant local binary pattern operator for efficient texture analysis," *Pattern Recognit. Lett.*, vol. 33, no. 9, pp. 1093–1100, 2012.

[19] F. M. Khellah, "Texture classification using dominant neighborhood structure," *IEEE Trans. Image Process.*, vol. 20, no. 11, pp. 3270–3279, Nov. 2011.

[20] J. Ren, X. Jiang, and J. Yuan, "Noise-resistant local binary pattern with an embedded error-correction mechanism," *IEEE Trans. Image Process.*, vol. 22, no. 10, pp. 4049–4060, Oct. 2013.

[21] S. Liao, Max W. K. Law, and Albert C. S. Chung, "Dominant local binary patterns for texture classification," *IEEE Trans. Image Process.*, vol. 18, no. 5, pp. 1107–1118, May 2009.

[22] M. Raja and V. Sadavisam, "Optimized local ternary patterns: A new texture model with set of optimal patterns for texture analysis," *J. Comput. Sci.*, vol. 9, no. 1, pp. 1–14, 2013.

[23] T. Mäenpää, M. Pietikäinen, "Multi-scale binary patterns for texture analysis," in *Proc. 13th SCIA*, 2003, pp. 885–892.

[24] T. Ahonen, J. Matas, C. He, and M. Pietikäinen, "Rotation invariant image description with local binary pattern histogram Fourier features," in *Proc. SCIA*, 2009, pp. 61–70.

[25] Z. Guo, L. Zhang, and D. Zhang, "A completed modeling of local binary pattern operator for texture classification," *IEEE Trans. Image Process.*, vol. 9, no. 16, pp. 1657–1663, Jun. 2010.

[26] H. Yang and Y. Wang, "A LBP-based face recognition method with Hamming distance constraint," in *Proc. 4th ICIG*, Aug. 2007, pp. 645–649.

[27] L. Liu, L. Zhao, Y. Long, G. Kuang, and P. Fieguth, "Extended local binary patterns for texture classification," *Image Vis. Comput.*, vol. 30, no. 2, pp. 86–99, Feb. 2012.

[28] T. Ahonen and M. Pietikäinen, "Soft histograms for local binary patterns," in *Proc. Finnish Signal Process. Symp.*, 2007.

[29] X. Tan and B. Triggs, "Enhanced local texture feature sets for face recognition under difficult lighting conditions," *IEEE Trans. Image Process.*, vol. 19, no. 6, pp. 1635–1650, Jun. 2010.

[30] A. Hafiane, G. Seetharaman, and B. Zavidovique, "Median binary pattern for textures classification," in *Proc. 4th ICIAR*, 2007, pp. 387–398.

[31] B. Caputo, E. Hayman, M. Fritz, and J.-O. Eklundh, "Classifying materials in the real world," *Image Vis. Comput.*, vol. 28, no. 1, pp. 150–163, 2010.

[32] P. Brodatz, *Textures: A Photographic Album for Artists and Designers*. New York, NY, USA: Dover, 1966.

[33] T. Ojala, T. Mäenpää, M. Pietikänen, J. Viertola, J. Kyllönen, and S. Huovinen, "Outex—New framework for empirical evaluation of texture analysis algorithms," in *Proc. 16th Int. Conf. Pattern Recognit.*, vol. 1. 2002, pp. 701–706.

[34] M. Pietikäinen, T. Ojala, and Z. Xu, "Rotation-invariant texture classification using feature distributions," *Pattern Recognit.* vol. 33, no. 1, pp. 43–52, Jan. 2000.

[35] Y. Zhao, D. Huang, and W. Jia, "Completed local binary count for rotation invariant texture classification," *IEEE Trans. Image Process.*, vol. 21, no. 10, pp. 4492–4497, Oct. 2012.

[36] L. Nanni, S. Brahnam, and A. Lumini, "A simple method for improving local binary patterns by considering nonuniform patterns," *Pattern Recognit.*, vol. 45, no. 10, pp. 3844–3852, 2012.

[37] Q. McNemar, "Note on the sampling error of the difference between correlated proportions or percentages," *Psychometrika*, vol. 12, no. 2, pp. 153–157, 1947.

[38] Z. Guo, L. Zhang, and D. Zhang, "Rotation invariant texture classification using LBP variance (LBPV) with global matching," *Pattern Recognit.*, vol. 43, no. 3, pp. 706–719, Mar. 2010.

[39] B. Caputo, E. Hayman, and P. Mallikarjuna, "Class-specific material categorization," in *Proc. 10th IEEE ICCV*, Beijing, China, Oct. 2005, pp. 1597–1604.

[40] J. Chen *et al.*, "WLD: A robust local image descriptor," *IEEE Trans. Pattern Anal. Mach. Intell.*, vol. 32, no. 9, pp. 1705–1720, Sep. 2010.

[41] C.-C. Chang and C.-J. Lin. (2001). *LIBSVM: A Library for Support Vector Machines* [Online]. Available: http://www.csie.ntu.edu.tw/ cjlin/libsvm

[42] P. Mallikarjuna, M. Fritz, A. T. Targhi, E. Hayman, B. Caputo, and J.-O. Eklundh. (2006). *The KTH-TIPS and KTH-TIPS2 Databases* [Online]. Available: http://www.nada.kth.se/cvap/databases/kth-tips/

[43] B. Schölkopf and A. Smola, *Learning With Kernels: Support Vector Machines, Regularization, Optimization and Beyond*. Cambridge, MA, USA: MIT Press, 2002.

Li Liu (M'12) received the B.S. degree in communication engineering, the M.S. degree in photogrammetry and remote sensing, and the Ph.D. degree in information and communication engineering from the National University of Defense Technology, Changsha, China, in 2003, 2005, and 2012, respectively. She joined the faculty at the National University of Defense Technology in 2012, where she is currently a Lecturer with the School of Information System and Management. During her Ph.D. study, she was a Visiting Student with the University of Waterloo, Waterloo, ON, Canada, from 2008 to 2010. She has held a visiting appointment at the Beijing University, Beijing, China. Dr. Liu is a Co-Chair of the International Workshop on Robust local descriptors for computer vision (RoLoD) at ACCV2014. Her current research interests include computer vision, texture analysis, pattern recognition, and video analysis and retrieval.

Yunli Long received the M.S. degree in electronic science and technology and the Ph.D. degree in information and communication engineering from the National University of Defense Technology, Changsha, China, in 2005 and 2012, respectively, where he is currently a Post-Doctoral Fellow with the School of Electronic Science and Engineering. His current research interests include object detection and recognition, object tracking, and video surveillance.

Paul W. Fieguth (S'87–M'96) received the B.A.Sc. degree in electrical engineering from the University of Waterloo, Waterloo, ON, Canada, in 1991, and the Ph.D. degree in electrical engineering from the Massachusetts Institute of Technology (MIT), Cambridge, MA, USA, in 1995. He joined the faculty at the University of Waterloo in 1996, where he is currently a Professor of Systems Design Engineering. He has held visiting appointments at the University of Heidelberg, Heidelberg, Germany, INRIA/Sophia, Nice, France, the Cambridge Research Laboratory, Boston, MA, USA, the University of Oxford, Oxford, U.K., and the Rutherford Appleton Laboratory, Oxfordshire, U.K., and post-doctoral positions in Computer Science at the University of Toronto, Toronto, ON, Canada, and in Information and Decision Systems at MIT. His research interests include statistical signal and image processing, hierarchical algorithms, data fusion, and the interdisciplinary applications of such methods, in particular, remote sensing.

Songyang Lao received the B.S. degree in information system engineering and the Ph.D. degree in system engineering from the National University of Defense Technology, Changsha, China, in 1990 and 1996, respectively. He joined the faculty at the National University of Defense Technology in 1996, where he is currently a Professor with the School of Information System and Management. She was a Visiting Scholar with the Dublin City University, Dublin, Ireland, from 2004 to 2005. His current research interests include image processing and video analysis, and human–computer interaction.

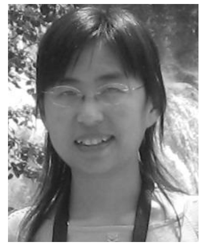

Guoying Zhao (SM'12) received the Ph.D. degree in computer science from the Chinese Academy of Sciences, Beijing, China, in 2005. She is currently an Associate Professor with the Center for Machine Vision Research, University of Oulu, Finland, where she has been a researcher since 2005. In 2011, she was selected to the highly competitive Academy Research Fellow position. She has authored or co-authored more than 100 papers in journals and conferences, and has served as a reviewer for many journals and conferences. She has lectured tutorials at ICPR 2006, ICCV 2009, and SCIA 2013, and authored/edited three books and two special issues in journals. Dr. Zhao was a Co-Chair of the International Workshop on Machine Learning for Vision-based Motion Analysis (MLVMA) at ECCV2008, ICCV2009, and CVPR2011, and of a special session for IEEE International Conference on Automatic Face and Gesture Recognition 2013. She is the co-organizer of ECCV2014 workshop on "Spontaneous Facial Behavior Analysis: Long term continuous analysis of facial expressions and micro-expressions" and INTERSPEECH 2014 special session on "Visual Speech Decoding". She is Member of program committees for many conferences, e.g. ICCV, CVPR, FG, BMVC, CRV, AVSS. She is IEEE Senior Member, and Editorial Board Member of International Journal of Applied Pattern Recognition and International Scholarly Research Network. Her current research interests include image and video descriptors, gait analysis, dynamic-texture recognition, facial-expression recognition, human motion analysis, and person identification.